SMALL, INEXPENSIVE COMBINED NO_x AND O_2 SENSOR

DE-FC26-02AL67632

FINAL REPORT

September 8, 2008

W. N. Lawless
C. F. Clark, Jr.

CeramPhysics, Inc.
921 Eastwind Drive
Suite 110
Westerville, Ohio 43081
614-882-2231 (office)
614-882-1437 (fax)
cpi@infinet.com

TABLE OF CONTENTS

I. SUMMARY

It has been successfully demonstrated in this program that a zirconia multilayer structure with rhodium-based porous electrodes performs well as an amperometric NO_X sensor. The sensitivity of the sensor bodies operating at 650 to 700 C is large, with demonstrated current outputs of 14 mA at 500 ppm NO_X from sensors with 30 layers. The sensor bodies are small (4.5 x 4.2 x 3.1 mm), rugged, and inexpensive. It is projected the sensor bodies will cost $5 - $10 in production. This program has built on another successful development program for an oxygen sensor based on the same principles and sponsored by DOE. This oxygen sensor is not sensitive to NO_X.

A significant technical hurdle has been identified and solved. It was found that the 100% Rh electrodes oxidize rapidly at the preferred operating temperatures of 650 - 700 C, and this oxidation is accompanied by a volume change which delaminates the sensors. The problem was solved by using alloys of Rh and Pt. It was found that a 10%/90% Rh/Pt alloy dropped the oxidation rate of the electrodes by orders of magnitude without degrading the NO_X sensitivity of the sensors, allowing long-term stable operation at the preferred operating temperatures.

Degradation in the sensor output caused by temperature cycling was identified as a change in resistance at the junction between the sensor body and the external leads attached to the sensor body. The degradation was eliminated by providing strong mechanical anchors for the wire and processing the junctions to obtain good electrical bonds.

The NO_x sensors also detect oxygen and therefore the fully-packaged sensor needs to be enclosed with an oxygen sensor in a small, heated zirconia chamber exposed to test gas through a diffusion plug which limits the flow of gas from the outside. Oxygen is pumped from the interior of the chamber to lower the oxygen content and the combination of measurements from the NO_X and oxygen sensors yields the NO_X content of the gas.

Two types of electronic control units were designed and built. One control unit provides independent constant voltages to the NO_X and oxygen sensors and reads the current from them (that is, detects the amount of test gas present). The second controller holds the fully-assembled sensor at the desired operating temperature and controllably pumps excess oxygen from the test chamber.

While the development of the sensor body was a complete success, the development of the packaging was only partially successful. All of the basic principles were demonstrated, but the packaging was too complex to optimize the operation within the resources of the program. Thus, no fully-assembled sensors were sent to outside labs for testing of cross-sensitivities, response times, etc.

Near the end of the program, Sensata Technologies of Attleboro, MA tested the sensor bodies and confirmed the CeramPhysics measurements as indicated in the following attached letter. Sensata was in the process of designing their own packaging for the sensor and performing cross-sensitivity tests when they stopped all sensor development work due to the automotive industry downturn. Recently Ceramatec Inc. of Salt Lake City has expressed an interest in testing the sensor, and other licensing opportunities are being pursued.

Sensata

Sensata Technologies
529 Pleasant Street
Attleboro, MA 02703
www.sensata.com

Mr Fred Clark
Ceramic Physics Inc
90 Eastwind Drive
Suite #110
Westerville OH 43081

DATE: May 27, 2008

SUBJECT: Department of Energy (NREL) Project DE-FC26-02AL67632, "Small, Inexpensive Combined NOx and O2 Sensor"

Dear Fred,

During Sensata Technologies' informal evaluation of your Oxygen and NOx multi-layered sensor cells we were pleased to confirm similar test results to what you reported. The large sensitivity of your sense elements and the potential to not require a reference gas provides unique opportunities for sensor control and packaging. Leveraging the high volume SMT capacitor manufacturing techniques in producing the sense elements should enable a relatively favorable cost structure vs. a single lab sense element construction approach. From our limited knowledge, this technology and the materials used are capable of working within an automotive exhaust system though further work would be needed to achieve a reliable and cost effective package for high volume applications.

Sincerely,
Pete Fracchiolla

Automotive Sensor Products
Design Engineering Supervisor
Senior Member Technical Staff

II. BACKGROUND AND DESCRIPTION OF THE SENSOR

The measurement of the oxygen partial pressure in exhaust gases has long been recognized as an important diagnostic for the efficient combustion of fossil fuels. In recent years the importance of NO_x in exhaust gases has gained increasing attention for emissions control, and regulatory agencies at both the state and federal levels have mandated reductions in NO_x levels.

In the automotive area, the Compression-Ignition, Direct-Injection (CIDI) engine holds great promise for achieving up to three times the fuel economy of comparable conventional vehicles by taking advantage of the high efficiency of the CIDI engine in a hybrid electric vehicle. These CIDI engines must, however, meet the same future emissions standards while offering the same level of performance and safety at the cost of today's comparable vehicles. The primary technical barrier facing automotive CIDI engines is the development of combustion control and emissions control technologies that are able to reliably meet stringent emissions regulations.

On-board sensors are an enabling technology for the implementation of combustion control and emissions control systems, and the focus of CIDI sensor research is on NO_x, particulate matter, and oxygen sensors, in that order of priority.

This program builds on a recent, very successful DOE program on a miniature, amperometric, zirconia oxygen sensor (DOE Inventions and Innovation program, DE-FG36-99GO10411), and this sensor will be described first in order to understand the NO_x sensor.

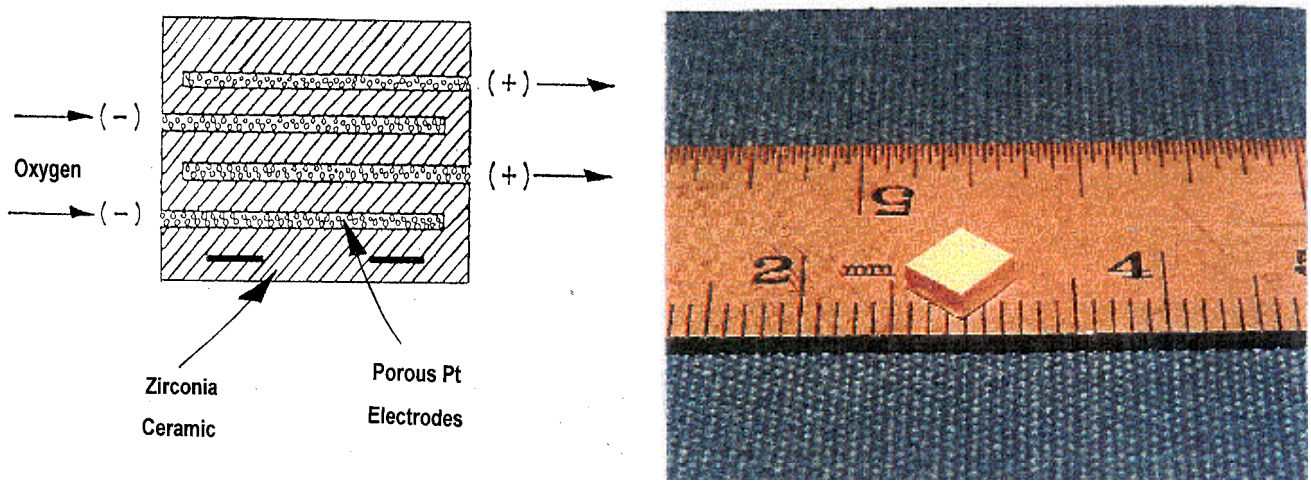

(a) (b)

FIGURE II-1. (a) Schematic illustration of the capacitor-type amperometric oxygen sensor showing the porous Pt electrodes for oxygen sensing. (b) Photograph of a manufactured integrated sensor body.

This sensor has the multilayer-ceramic-capacitor structure illustrated schematically in Fig. II-1(a) and consists of ceramic zirconia layers separated by porous Pt electrodes. Under a voltage applied to the electrodes, oxygen is "pumped" from the (-) cathodes to the (+) anodes through the ceramic layers, and this pumping or amperometric current provides a measure of the oxygen partial pressure in the surrounding gas. The tortuous diffusion paths through the porous Pt electrodes provide the diffusion-limitation for amperometric oxygen sensing.

A photograph of a manufactured sensor body is shown in Fig. II-1(b). There are 11 ceramic sensing layers in this sensor each of thickness 0.070 cm. This sensor has the economic advantage of being inexpensively manufacturable in large volumes using well-established capacitor-manufacturing methods and facilities. The capacitor manufacturer has estimated a manufacturing cost of $5 - $10 per sensor body in large volumes.

The response time of the sensor is very fast. An attempt to measure the response time in a "bursting balloon" experiment put an upper limit on the response time of 40 ms at 800 ºC.

One source of long-term changes in oxygen sensors is slow sintering of the Pt electrode material. Rosemount Analytical, Inc has developed a proprietary method for stabilizing Pt electrodes and it was found that this method worked well to stabilize the electrodes in the multilayer oxygen sensors.

We now consider how this sensor can be used to measure the NO_x content of exhaust gases. First, it is well-known that Rh catalyzes the decomposition of NO_x into N_2 and O_2, but Pt (and, more particularly, Pt/Au) does not. Therefore, replacing the porous Pt electrodes in the sensor with porous Rh electrodes, the NO_x in the surrounding gas would be decomposed on these electrodes and the released oxygen would constitute an amperometric current under an applied voltage. In this fashion, the amperometric current provides a measure of the NO_x by measuring the oxygen content of the NO_x.

Things are not this simple, however, because the surrounding gas may also contain oxygen, and this "background" oxygen content may be much larger than the released oxygen from the NO_x and has to be taken into account.

The proposed device to accomplish these sensing functions is shown schematically in Fig. II-2. A zirconia tube or shell has an open end exposed to the exhaust gas through a diffusion plug, and an oxygen sensor (not shown) as described above may be mounted in the exhaust gas at this open end of the tube. Separate O_2 and NO_x sensors are sealed into the interior at the other end of the tube and mounted on a solid plug with holes for electrical feedthrus. In Fig. II-2, the plugs are shown outside the zirconia shell. After assembly they are sealed against the shoulders on the inside of the shell.

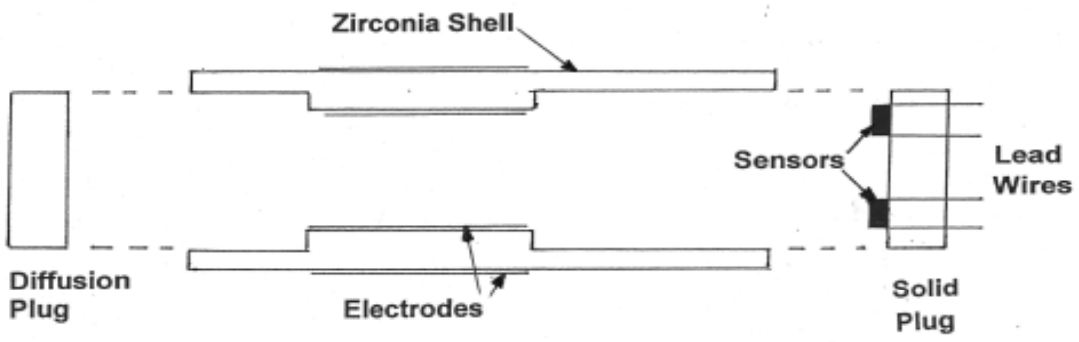

FIGURE II-2. Schematic illustration of the proposed fully-assembled sensor for measuring the oxygen partial pressure and the NO_x content of an exhaust gas.

The center portion of the Zirconia Tube is electroded with an internal Pt/Au cathode electrode (to prevent NO_x decomposition on this electrode) and an external Pt anode electrode. A voltage

applied across these electrodes causes the oxygen within the tube to be pumped to a low level in order to improve the NO_x discrimination by the two sensors mounted on the solid plug. A heater (not shown) is wrapped on the outside of the tube. There is no need for a reference gas, and the device is mounted directly in the exhaust gas. For mounting, a flange would be attached at the end with the lead wires. Also not shown are an insulation layer and particulate and other filters common to all exhaust sensors.

The zirconia diffusion plug plays the important role of diffusion-limiting the amount of exhaust gas entering the interior of the tube thereby ensuring that a very low level of oxygen is maintained in the interior of the tube by the pumping process. The overall size of the package illustrated in Fig. II-2 is expected to be about 0.5" outside diameter and 2" long.

The operation of the device is as follows: The assembly is self-heated to the operating temperature (e.g., 700 - 750 ºC), and the external oxygen sensor measures the oxygen partial pressure in the exhaust gas. A voltage applied to the electrodes on the zirconia tube pumps the oxygen in the interior of the tube to a very low level, and the internal O_2 sensor measures this low oxygen level. The NO_x sensor measures ***both*** this low oxygen level ***and*** the oxygen from the NO_x decomposition, and these two measurements from the two internal sensors are then used to determine the NO_x content.

Although not shown here, the multilayering manufacturing process has the flexibility of producing layers electroded with Pt/Au and separate layers electroded with Rh in the same sensor body.

A feedback feature in the instrumentation is possible. Namely, using the oxygen measurement from the internal O_2 sensor, the rate of pumping oxygen out of the tube interior could be adjusted to hold the internal oxygen content constant and therefore to improve the accuracy of the NO_x measurement and to conserve power by pumping out no more oxygen than necessary.

There were two separate Phases to this program. All the development work was originally planned to take place within the initial Phase I. However, numerous technical problems were encountered, as described below. In particular, recognition that pure rhodium electrodes oxidized led to shifting resources to solving this problem. Phase II provided additional DOE funds to complete the work on the electrodes and to pursue development of the fully packaged sensor. In the end the oxidation problem was fully and successfully solved, but the completion of the packaging of all the other sensor elements was not completed. Even the resources available from Phase II were insufficient to solve all the packaging problems. The best that could be done was to demonstrate that the operating principles of the packaged sensor are correct and to develop engineering designs for a manufacturable sensor.

III. DESCRIPTION OF EQUIPMENT/MEASURING SYSTEM

The sensor test facilities consist of a measurement probe inserted into an oven, a gas handling system, a data collection system, and two controllers. The first controller was built and tested in the first phase of this program by a subcontractor and provides a constant voltage input to each of three sensors (one NO_x and two O_2 sensors) envisioned for the final, fully-assembled sensor. There are three sections to this controller providing variable independent voltages to each sensor. The second controller was developed by the same subcontractor during the second phase of the program and has a temperature control section and an oxygen pump control section. Each of these will be described below in detail.

The sensor bodies are measured in a probe designed and built specifically for these sensors as shown in Fig. III-1. This probe is inserted into a stainless steel shell 0.75" in diameter and approximately 15" long. This tube is kept small to minimize the flush time when the NO_x partial pressure concentration is changed. The shell is inserted horizontally into an oven as shown in Fig. III-2, exiting the oven through a hole in the front wall. The shell is sealed on the inside end and is flanged on the outside end. The shell has a gas exit tube welded into the hot end, and this exit-port tube also exits through the front of the oven. There is a port for input gas through the front flange of the platform. A sealed port for a thermocouple and a sealed electrical connector for eight lead wires also enter through this same flange.

The gas flow system has three cylinders of gas: nitrogen with 500 ppm NO_x, nitrogen with 20 ppm NO_x, and pure nitrogen (with about 3 - 5 ppm of oxygen). The cylinders with NO_x are valved in parallel so one or the other can be selected and mixed with the pure nitrogen. Mixing is done with two MKS flow controller/measurement instruments, Model 1159B, which are in turn each controlled with a 0-5 VDC signal from dual power supplies (HP Model 6211).

Primary control of the NO_x content of the gas is achieved by careful control of the mixing ratios using the flow controllers. The total combined flow from the two tanks is kept constant while the ratio of flows is changed.

From the flow controllers, the mixed gas flows directly into the sensor probe described above. The gas flow is heated on flowing into the oven and is at oven temperature by the time it reaches the sensor at the hot end of the probe. After the gas exits the probe, it goes directly into one of two commercial gas analyzers. A Thermox Ametek oxygen measurement system with a standard zirconia tube is used to make a Nernst measurement of the oxygen in the gas stream.

During the first phase of this program, the NO_x measurements were made with an electrochemical NO_x sensor made by EIT with a sensitivity of 0-500 ppm NO_x. This sensor is relatively inexpensive compared to chemiluminescent measurement instruments and does respond to changes in NO_x. However, it was found that this commercial sensor has a long stabilization time when first turned on, drifts (both zero point and span) over hours, and is slow to respond. Therefore it is impractical to rely on this sensor for a comparative NO_x measurement. During the second phase of the program a California Analytical Instruments Model 600 CLD chemiluminescent detector was purchased to increase the accuracy of the primary NO_x measurements. The span of this instrument was periodically checked using gas with a known NO_x content (either 20 ppm or 500 ppm in N_2)

The sensor to be tested is attached electrically to four platinum wires which run from the sealed electrical connector on the front flange to the hot end of the probe where the sensor is

Figure III-1

Figure III-2

located. The wires are kept electrically isolated within mullite thermocouple tubes anchored to the platform. When the Pt wires exit these tubes near the sensor, they are combined into two twisted pairs and the short gold wires bonded to sensor are wrapped on these twisted pairs and bonded with fired-on gold paste. Using twisted pairs near the sensor eliminates as much lead resistance as possible from the measurement.

A sealed, K-type thermocouple enters through the front flange of the sensor probe platform (the yellow connector in Fig. III-2) and extends to the end of the probe near the sensor. The test sensor sits on an alumina sheet near the end of the platform. The oven temperature is controlled through a separate oven controller with a separate thermocouple in the oven holding the probe.

All relevant parameters are measured with Keithley Model 181 or 182 DVM's. Data are collected from these DVM's through a computer program accessing the DVM's over a IEEE-488 data link. Five different DVM's monitor the Thermox voltage, the internal probe thermocouple, the sensor voltage and current and the output of the commercial NO_x sensor.

A special power supply to control the applied voltage at the test sensor has been designed and built by RJS Electronics, Inc. of Columbus, OH. As discussed above, it is anticipated that the fully-packaged NO_x/O_2 sensor will consist of an external oxygen sensor to measure the oxygen content of the exhaust gas and NO_x and oxygen sensors internal to the zirconia shell. In anticipation of implementing this design, the power supply built by RJS consists of three independent power supplies contained in a single box. Output leads consist of excitation leads for current to each sensor and sense leads for reading the voltage near each sensor, as shown on the lower controller box in Fig. III-3. All three power supplies use a microprocessor and appropriate A/D converters cycling at less than a millisecond to read and constantly monitor and adjust voltage to each sensor. The final stage of regulation is done with an appropriate analog circuit.

For each sensor power supply, it is desired to monitor and hold constant the voltage across the sensor. The current flowing through the excitation leads are then monitored across a 1 ohm standard resistor in the power supply box and are a direct measure of either the NO_x or the oxygen in the test gas surrounding each sensor. Additional ports are provided for monitoring the sensor voltage.

Voltage changes for each sensor power supply are made through the communication port of a computer to the internal microprocessor using simple keyboard commands. The firmware contains current and voltage limit safeguards to protect the power supplies and the sensor.

The voltage applied to the sensor needs to be quite stable over the long-term to ensure the accuracy of the measurement. Figure III-4 shows the stability of the voltage output during an overnight run monitoring the long-term controller performance. As can be seen, the voltage is constant to within $\pm$ 0.005%. The Keithley Model 182 DVM monitoring the voltage is rated to about $\pm$ 0.0029% percent changes combining 24 hour drift and the temperature coefficient. Therefore, the power supply is constant to within about 0.0021%, which is excellent.

A second controller has also been built by RJS Electronics and is shown as the top controller box in Fig III-3. This controller has two functions, both associated with the fully-assembled sensor. First, it controls the temperature of the sensor by controlling the current output to a Kanthal heater wrapped on the sensor with feedback from a K-type thermocouple. The second function is controlling the oxygen partial pressure in the isolated zone inside the sensor. This zone contains both a NO_x and an O_2 sensor along with a pumping electrode to remove most oxygen. The controller senses the oxygen content from the output of one of the oxygen sensor


O2 heater / pump
temperature
heater
O2 pump
Power
Excitation Power Supply
O2 Voltage
O2 Current
O2 #1
O2 #2
Power

Figure III-3

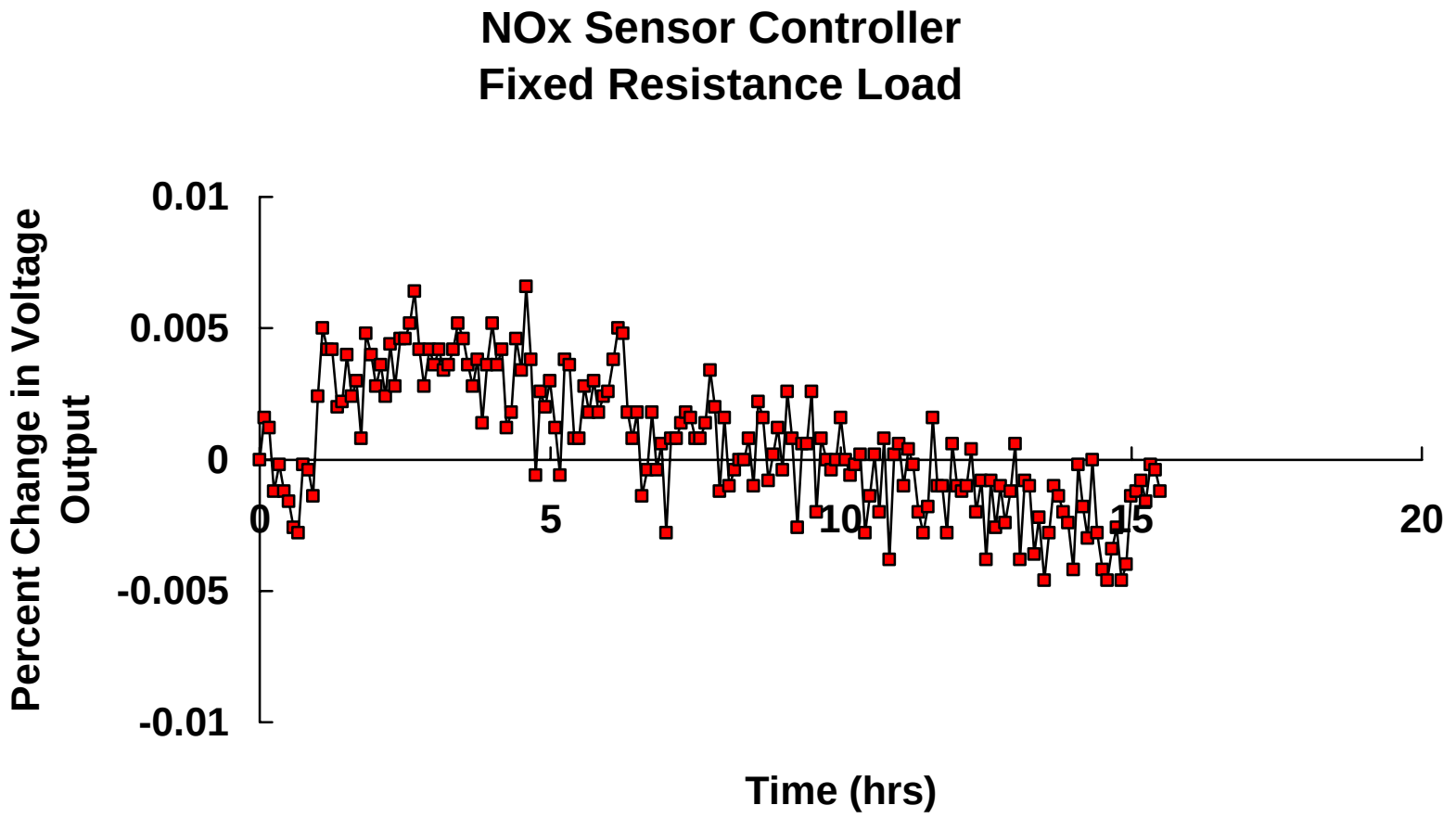
NOx Sensor Controller
Fixed Resistance Load
Percent Change in Voltage Output
0.01
0.005
0
-0.005
-0.01
0
5
10
15
20
Time (hrs)

Figure III-4

control sections of the first controller described above. This input controls the current to the pumping electrodes which remove oxygen from the inner space. As with the first controller, the set point of each of these functions is controlled through the communications port of a computer with simple keyboard commands.

IV. DEVELOPMENT OF THE CORE SENSOR BODY

Description of the Final Sensor Body

The development of the NO_x sensor body, the core sensing element, has been completely successful. Figure IV-1 is a photo of the final sensor configuration which consists of 30 active layers of 8% yttria-stabilized zirconia (YSZ), each with an area of 0.151" x 0.125" and a thickness of 0.0031". The electrodes are made of a porous alloy of 10% rhodium and 90% platinum (atomic ratio) and the preferred sintering temperature is 1150 °C. Final outside dimensions are 0.177" (L) x 0.164" (W) x 0.123" (H).

The sensors have been made with standard capacitor multilayer techniques by MRA Laboratories of Adams, MA. The production method has a number of advantages including low cost for quantity production, reproducibility, ruggedness, and good quality control.

The preferred operating temperature for the sensor is 650 °C to 700 °C and the preferred applied voltage is 0.5 V. Under these operating conditions, the sensor has a linear response of 28 microamps per ppm of NO_x over the range of 0 to 500 ppm (see Fig. IV-16 below). That is, at 500 ppm of NO_x, the output current is 14 milliamps, a very large value compared to other amperometric NO_x sensors.

To attach lead wires for tests in this program, thin layers of platinum and gold pastes are applied in narrow stripes along one side of each face with exposed electrodes. These layers electrically connect all the layers and provide pads to attach small (0.004" - 0.005" diameter) gold wires to each face. This leaves most of the face open to the surrounding atmosphere. The wires are attached with a thicker layer of gold paste. The wires wrap around the corners of the sensor body above and below the attachment pads and on these faces, the wire is held in place using a small dab of Aremco 516, a bonding material that matches the thermal expansion of the zirconia bodies. These anchors provide mechanical stability to the wires.

Sensor Body Development

In order to complete the successful development of the sensor body described above, two major problems needed to be solved: oxidation of rhodium at elevated temperatures, and poor electrical and mechanical contacts where external wires are joined to the sensor bodies. A thorough description of each of these problems and its solution is presented below. The final subsection below describes the results of the tests made on the sensor bodies once the problems were solved.

For most of the program, sensors with only three active layers (four electrodes) were used for testing in order to minimize costs. After the final selection of electrode material was made, sensors with 20 layers were made, followed by sensors with the final configuration of 30 layers. MRA feels that 30 layers is about the upper limit of layers that can be stacked and dried within reasonable time/temperature restraints. The sensitivity (mA/ppm of NO_x) of the sensor should be proportional to the number of layers, and this was found to be true. Therefore 30 layers was maintained as the final sensor configuration.

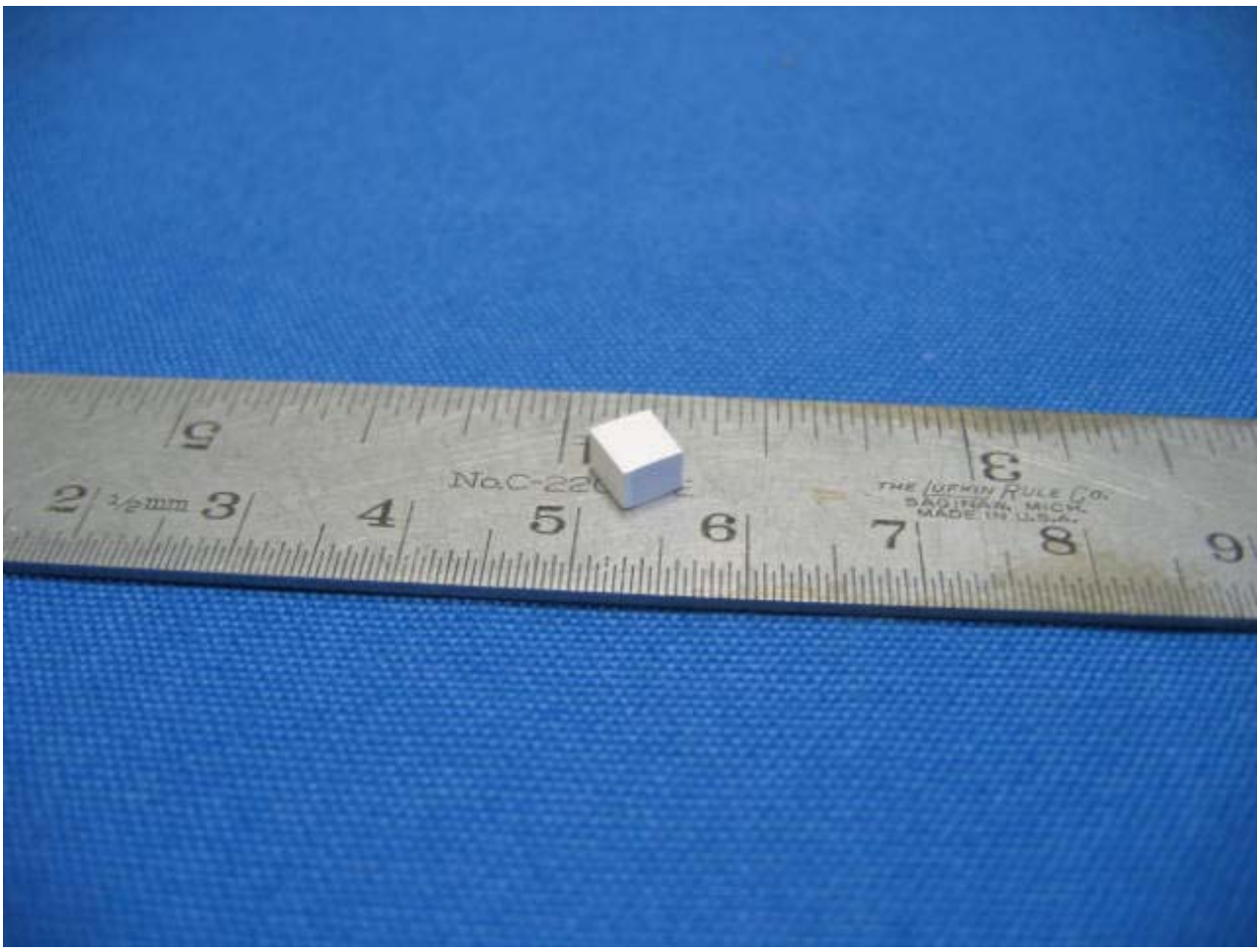

Figure IV-1

Electrode Oxidation Problem and Resolution

The first sensors in the program were made by MRA with 100% rhodium electrodes. The first tests were with sensors sintered at 1250 °C for three hours and were tested successfully. As shown in Fig. IV-2, the first tests were made at 775, 800, and 825 °C, typical of the operating temperature of the companion oxygen sensors. However, not long into testing, the sensors starting delaminating along planes defined by the electrodes. Subsequently, MRA found that rhodium, unlike platinum, oxidizes below 1000 °C.

The oxidation rate is relatively slow and peaks around 800 °C which is undesirable since the preferred operating temperatures is 800 °C or less. The rate of oxidation decreases with temperature below 800 °C. Oxidation of rhodium is accompanied by a volume increase of 86% and it is this volume change that delaminated the sensors.

Three possible solutions to the oxidation problem were considered. First, since oxidation is a thermally-activated process, the operating temperature might be lowered enough to effectively eliminate the problem without compromising the sensor response. A number of sensor tests were made at temperatures between 450 and 650 °C, and while the sensor still detected NO_x, the sensitivity was too low.

The second possible solution was to always keep the NO_x sensor in a reducing atmosphere. This was considered possible because of calculations of the equilibrium constant for the oxidation of rhodium as a function of temperature:

$$K = \exp(-\Delta F/RT) \qquad \text{Eq. IV-1}$$

where K is the equilibrium constant, ΔF is the free energy of formation, R is the gas constant, and T is the absolute temperature. K is in turn related to the equilibrium oxygen partial pressure, that is, the O_2 equilibrium partial pressure between reduction and oxidation. There are three oxides of rhodium, Rh_2O, RhO, and Rh_2O_3 (listed in order of decreasing stability). From handbook values of the free energy of formation for each of these oxides and Eq. IV-1, the equilibrium oxygen partial pressure can be calculated and is shown as a function of temperature in Fig. IV-3.

These equilibrium pO_2's are large enough to consider maintaining the sensors in a low pO_2 atmosphere by continually pumping the zirconia shell to prevent rhodium oxidation. As an example, at 727 °C (1000 K), Rh_2O_3 will reduce to RhO below oxygen partial pressures of 0.049 atm. RhO will reduce to Rh_2O at oxygen partial pressures below 0.18 atm. Finally, Rh_2O will reduce to Rh at oxygen partial pressures below 3.4 E-5 atm. It is feasible to think of pumping the oxygen in the zirconia shell of the sensor below this pressure.

However, there are problems with this solution. First, even though the equilibrium oxygen concentration is defined by Eq. IV-1, the kinetics of the reduction reactions are unknown. That is, even if the rhodium oxides would reduce, the rate of reduction might be slow. Second, it would be hard under all conditions to make sure that the atmosphere inside the zirconia shell was always maintained at a low enough oxygen partial pressure to ensure the rhodium was always reduced.

The third and successful solution to the oxidation problem was based on the observation that a type R thermocouple is composed of Pt/13%Rh vs Pt and a type B thermocouple is

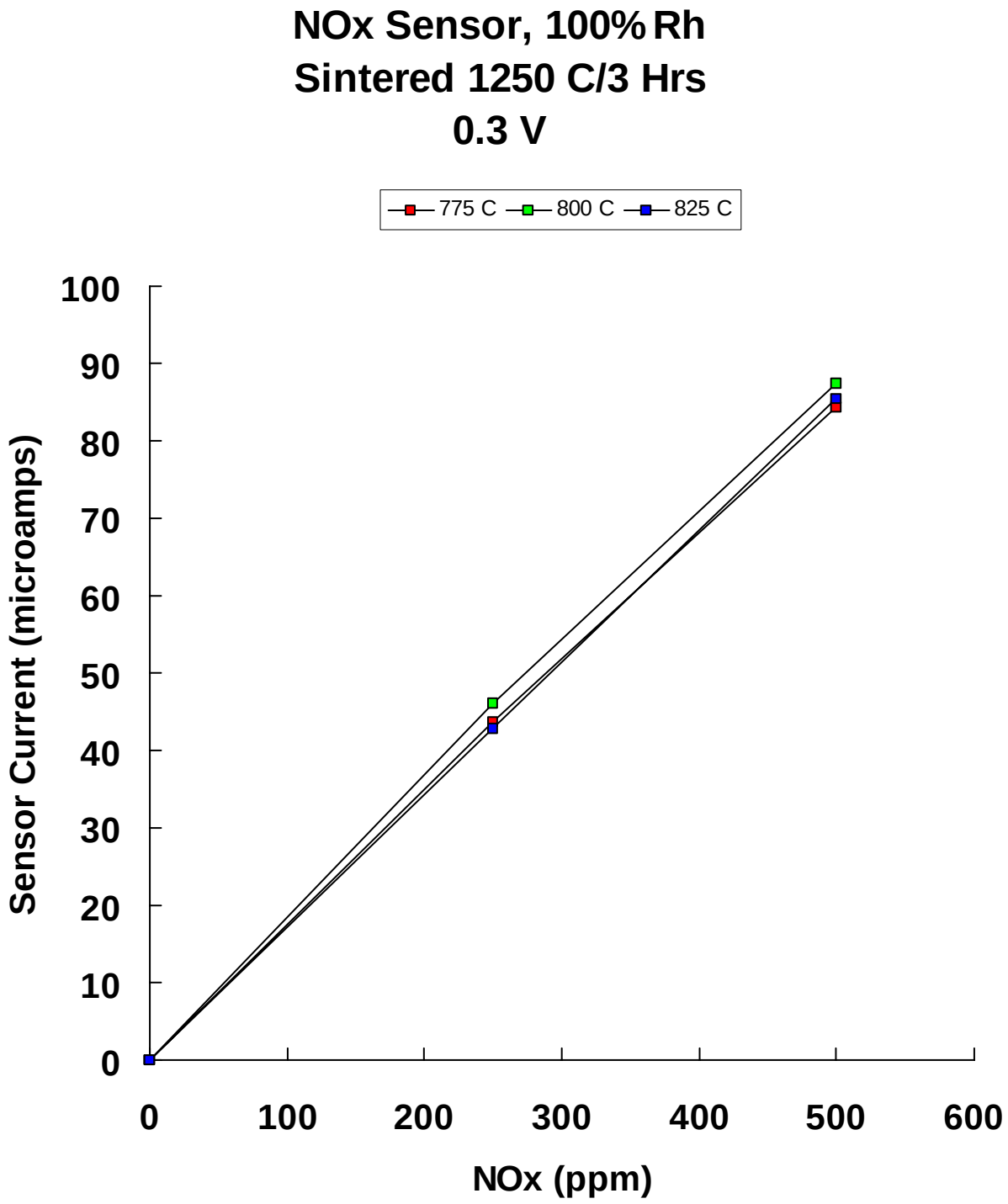
NOx Sensor, 100% Rh
Sintered 1250 C/3 Hrs
0.3 V
775 C
800 C
825 C
Sensor Current (microamps)
100
90
80
70
60
50
40
30
20
10
0
0
100
200
300
400
500
600
NOx (ppm)

Figure IV- 2

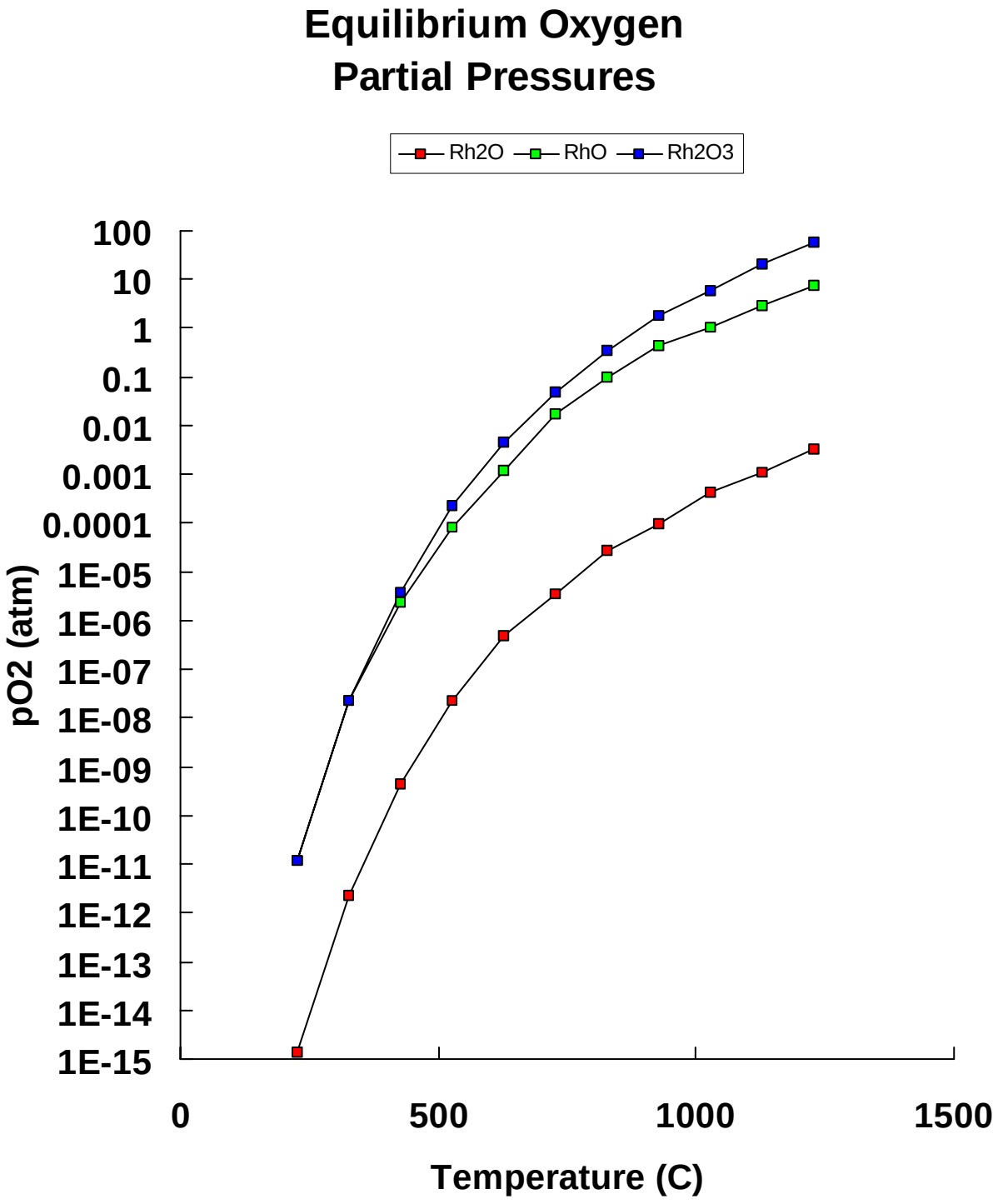
Equilibrium Oxygen
Partial Pressures
Rh2O
RhO
Rh2O3
100
10
1
0.1
0.01
0.001
0.0001
1E-05
1E-06
1E-07
1E-08
1E-09
1E-10
1E-11
1E-12
1E-13
1E-14
1E-15
pO2 (atm)
0
500
1000
1500
Temperature (C)

Figure IV-3

composed of Pt/30%Rh vs Pt/6%Rh and both thermocouples are rated to work well above 800 °C in air, implying that there are solid solutions of Pt and Rh which do not oxidize. However, knowing that a solid solution of Rh and Pt will not oxidize does not guarantee that the alloy will still catalyze NO_x or the sensor will retain sufficient sensitivity. Also unknown was the oxidation rate of these solid solutions.

Thus, if mixtures of Pt and Rh were to be the answer, the following questions had to be answered: (1) Does the oxidation rate of Rh/Pt alloys decrease with increasing Pt content?, and (2) Do solid solutions of Rh and Pt compromise NO_x catalysis and thus the sensor sensitivity?

To answer these questions, sensors were made with electrodes of 75%/25% Rh/Pt and 50%/50% Rh/Pt in the first phase of this program. In the second phase of the program, sensors were made where the Rh content of the electrodes was decreased in steps of 10% from 50%/50% Rh/Pt to 10%/90% Rh/Pt. The results of these tests are shown below.

Measuring the oxidation rate was based on the following approach. Since the rhodium oxides are not metallic conductors, a measure of the change in resistance of the Rh electrodes with time is a measure of the oxidation rate. For each Rh/Pt electrode ratio, MRA removed the pullbacks on the sensor bodies by grinding off the material at the ends of a couple of multilayer sensors, exposing all the electrodes on each face. Leads were attached to these "resistors" and placed into the NO_x sensor measuring apparatus. The resistance was measured in air as a function of time (~ tens of hours), temperature, and sintering temperature (increasing the sintering temperature decreases the porosity of the electrodes, thus slowing the oxygen transport through the electrodes).

The data on the electrode resistance as a function of time were analyzed by assuming that the rate of oxidation of rhodium atoms is described by a first-order rate equation:

$$dn/dt = kn \text{ or } n = n_0\exp(kt)$$

where n is the number of oxidized atoms and is thus assumed to be proportional to the resistance R and where

$$k = k_0\exp(-Q/T)$$

where Q is an activation energy and T is temperature in Kelvin. A Taylor expansion of the first equation for small values of kt yields

$$d(R/R_0)/dt = B\exp(-A/T) \qquad \text{Eq. IV-2}$$

Therefore an Arrhenius plot of the log of the rate of oxidation $\ln[d(R/R_0)/dt]$ versus 1/T would give a straight line and this was found to be true experimentally to a reasonable accuracy.

The procedure to analyze oxidation rates was to heat the sensor "resistors" described above to a particular temperature and hold at that temperature for 10-20 hours, then repeat this procedure at other temperatures. Using the average resistance at any one temperature as R_0, $d(R/R_0)/dt$ was calculated as the average percentage change in R per hour. The data from each temperature was then plotted on an Arrhenius plot for comparison with other data and for calculation of the fitting constants A and B in Eq. IV-2.

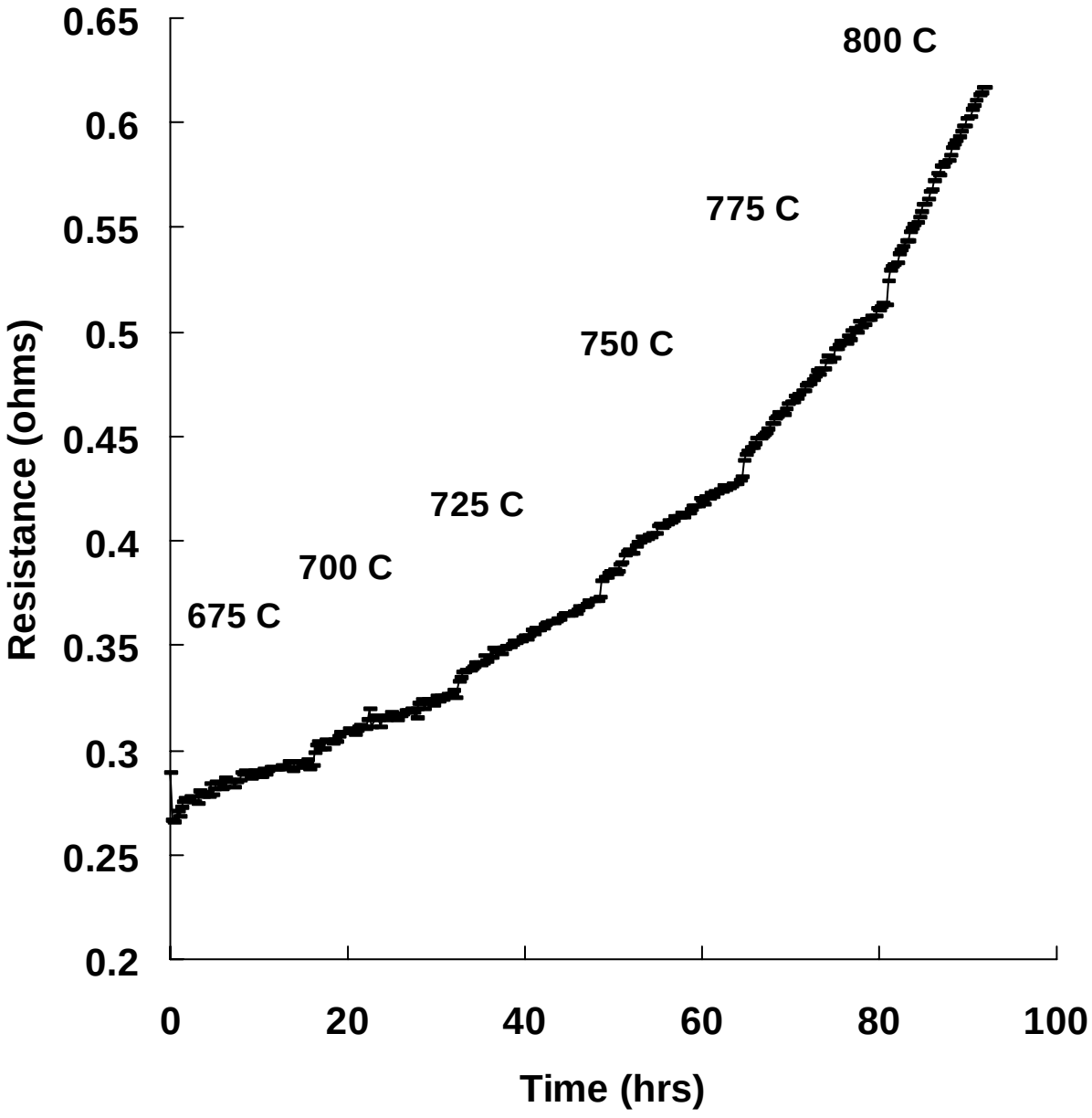
Oxidation Rate, 75/25 Rh/Pt
Sintered 1225/3, T from 675 C
to 800 C in 25 C Steps
Resistance (ohms)
0.65
0.6
0.55
0.5
0.45
0.4
0.35
0.3
0.25
0.2
0
20
40
60
80
100
Time (hrs)
675 C
700 C
725 C
750 C
775 C
800 C

Figure IV-4

An example of measured resistance versus time data for 75%/25% Rh/Pt electrodes is shown in Fig. IV-4 where the temperature was held progressively at six different levels at 25 °C intervals from 675 to 800 °C. These correspond to the six regions on the graph, each with a different slope. As can be seen, the rate of oxidation increased as the temperature increased, that is, the slopes increased. These data were then reduced according to Eq. IV-2 in order to compare them to other sensors with different sintering temperatures and different Rh/Pt ratios.

Figure IV-5 shows the change in oxidation rate for three sensors with the three different Rh/Pt ratios measured in Phase I of the program. All sensors were sintered at 1200 °C for 3 hrs and, as hoped, the oxidation rate drops significantly as the Pt content increases.

Figure IV-6 shows the change in oxidation rate as a function of sintering temperature for sensors with a 75%/25% Rh/Pt ratio. Increasing the sintering temperature decreases the porosity of the electrodes thus decreasing the diffusion rate of gas into the electrodes. It would be expected that the oxidation rate would drop with increasing sintering temperature and this is, in fact, what is found. This same trend holds for the sensors with 50%/50% Rh/Pt electrodes.

In Phase I, an attempt was made to correlate the change in sensitivity with increasing oxidation. A sensor with 75%/25% Rh/Pt electrodes was alternately exposed to air at elevated temperatures for fixed periods of time and tested for NO_x sensitivity. The exposure time in air was enough to increase the oxidation by several hundred percent as derived from the measured rate. There was no change in sensitivity that could be clearly attributed to oxidation. This question is revisited below after the electrode tests in Phase II.

In Phase II of the program, the oxidation analysis continued with electrode Rh percentages of 50%, 30%, 20%, and 10%. An Arrhenius plot for the these electrodes is shown in Fig. IV-7 for sensors measured at a sintering temperature of 1175 °C. Note the change in slopes on this plot. For the 50%/50% Rh/Pt electrode, the oxidation rate goes up as the temperature goes up (as 1/T goes down). The slope for the electrodes with lower Rh contents are much flatter and reversed. There is a ready explanation for this. It is well-known that pure rhodium has a peak in the oxidation rate about 800 °C and the rate drops above this temperature. Over 1000 °C, rhodium reduces in air. In Fig. IV-7, the highest temperature used for the measurements was at 800 °C corresponding to the lowest points on the 1/T axis. If we were to measure the oxidation rate between 800 °C and 900 °C for the 50%/50% Rh/Pt electrodes, the slope of the curve in Fig. IV-7 would be in the same direction as the other slopes. Therefore, it is likely that alloying rhodium with platinum has shifted the temperature of maximum oxidation to lower temperatures, while simultaneously decreasing the over-all rate.

It is even possible that the oxidation/reduction characteristics of the alloy have been shifted enough that at the preferred operating temperature of 650 - 700 °C, the alloy will slowly reduce rather than oxidize at the low oxygen partial pressures normally encountered during measurements.

Another type of summary plot is shown in Fig. IV-8 where the oxidation rate is plotted as a function of rhodium content for three sintering temperatures at 750 °C. Again, the oxidation rate drops dramatically as the rhodium content decreases. The oxidation rate does not change much with sintering temperature, indicating that from the standpoint of oxidation rate any of these sintering temperatures can be used for the final selection of sensors.

The effect of the drop in oxidation rate is best illustrated with an example based on the data in Fig. IV-5 for sensors sintered at 1200 °C. For 100% rhodium electrodes, the time required at 600 °C for a 100% increase in resistance in the electrodes is about 0.0299 years or about 11 days.

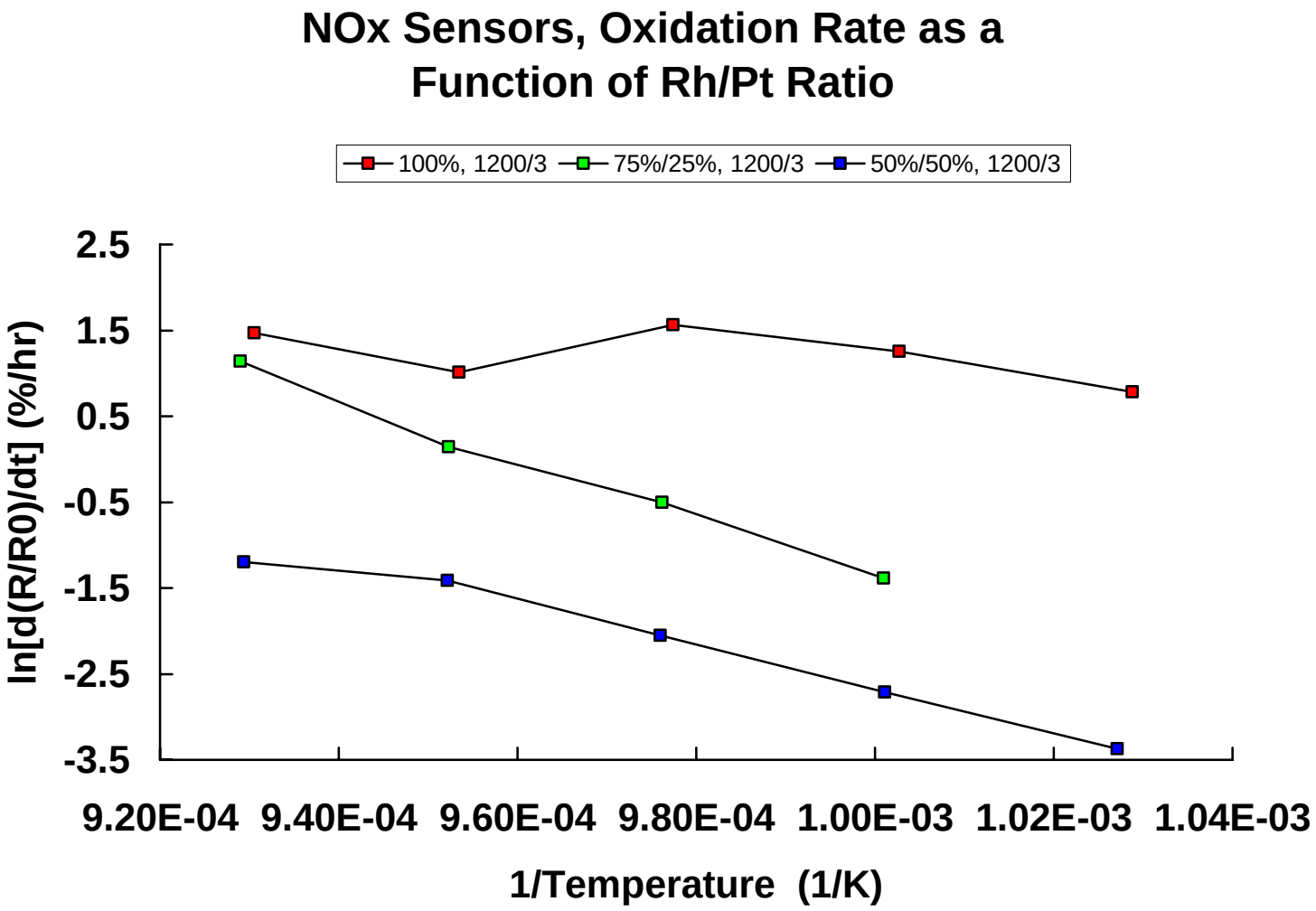
NOx Sensors, Oxidation Rate as a Function of Rh/Pt Ratio
100%, 1200/3
75%/25%, 1200/3
50%/50%, 1200/3
ln[d(R/R0)/dt] (%/hr)
2.5
1.5
0.5
-0.5
-1.5
-2.5
-3.5
9.20E-04
9.40E-04
9.60E-04
9.80E-04
1.00E-03
1.02E-03
1.04E-03
1/Temperature (1/K)

Figure IV-5

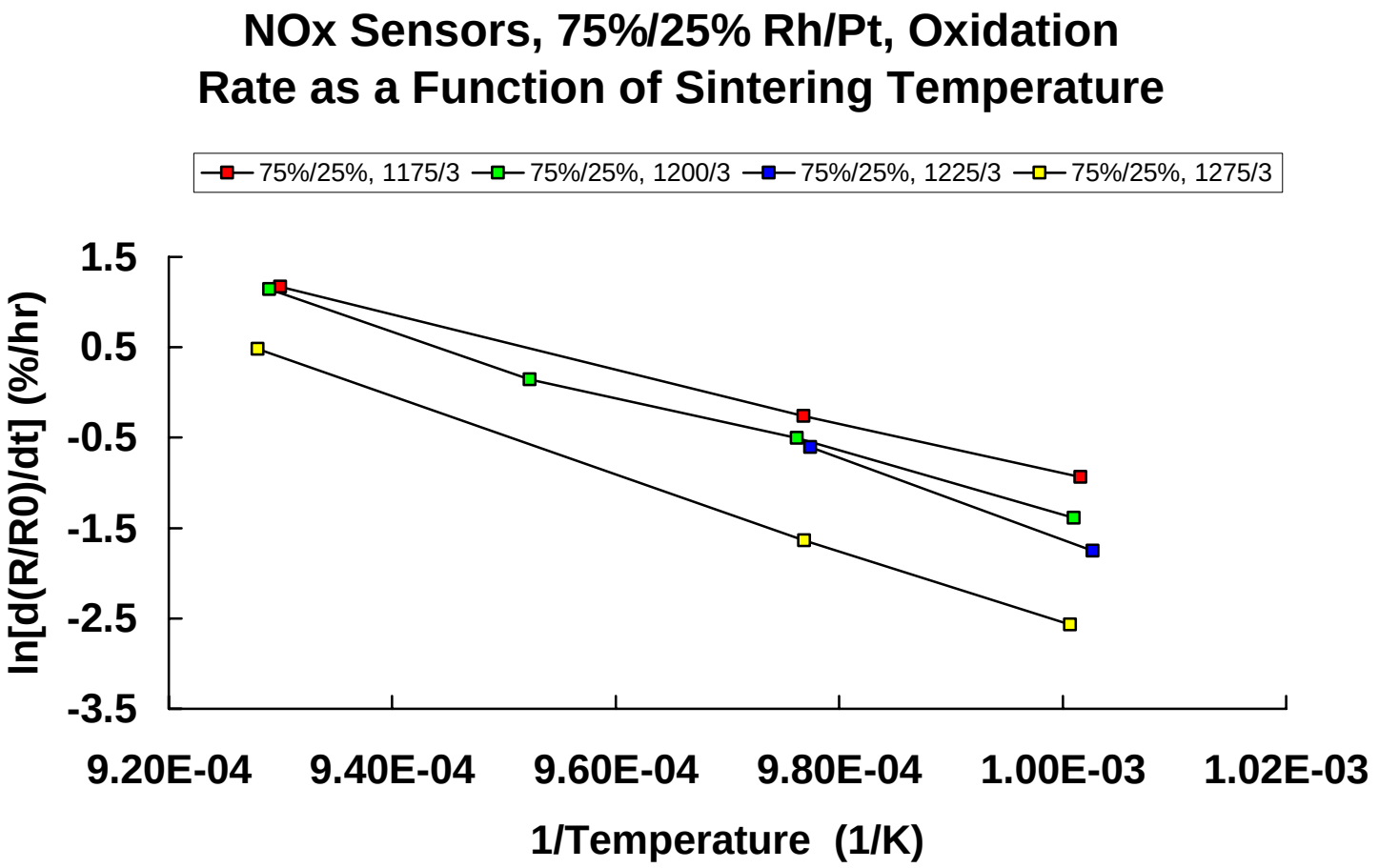
NOx Sensors, 75%/25% Rh/Pt, Oxidation Rate as a Function of Sintering Temperature
75%/25%, 1175/3
75%/25%, 1200/3
75%/25%, 1225/3
75%/25%, 1275/3
ln[d(R/R0)/dt] (%/hr)
1.5
0.5
-0.5
-1.5
-2.5
-3.5
9.20E-04
9.40E-04
9.60E-04
9.80E-04
1.00E-03
1.02E-03
1/Temperature (1/K)

Figure IV-6

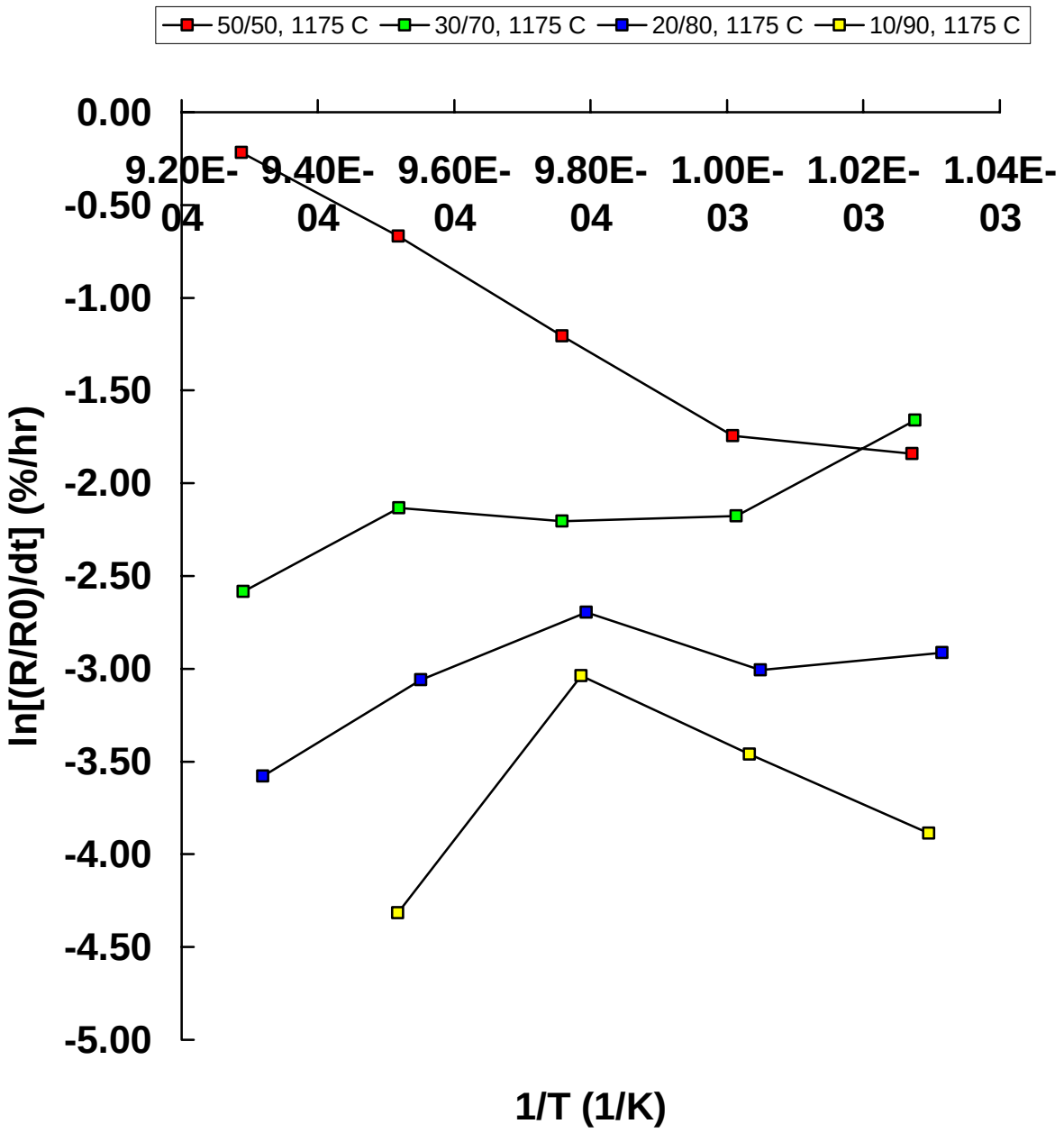
NOx "Resistors" Oxidation Rate
50/50, 1175 C
30/70, 1175 C
20/80, 1175 C
10/90, 1175 C
0.00
-0.50
-1.00
-1.50
-2.00
-2.50
-3.00
-3.50
-4.00
-4.50
-5.00
9.20E-04
9.40E-04
9.60E-04
9.80E-04
1.00E-03
1.02E-03
1.04E-03
ln[(R/R0)/dt] (%/hr)
1/T (1/K)

Figure IV-7

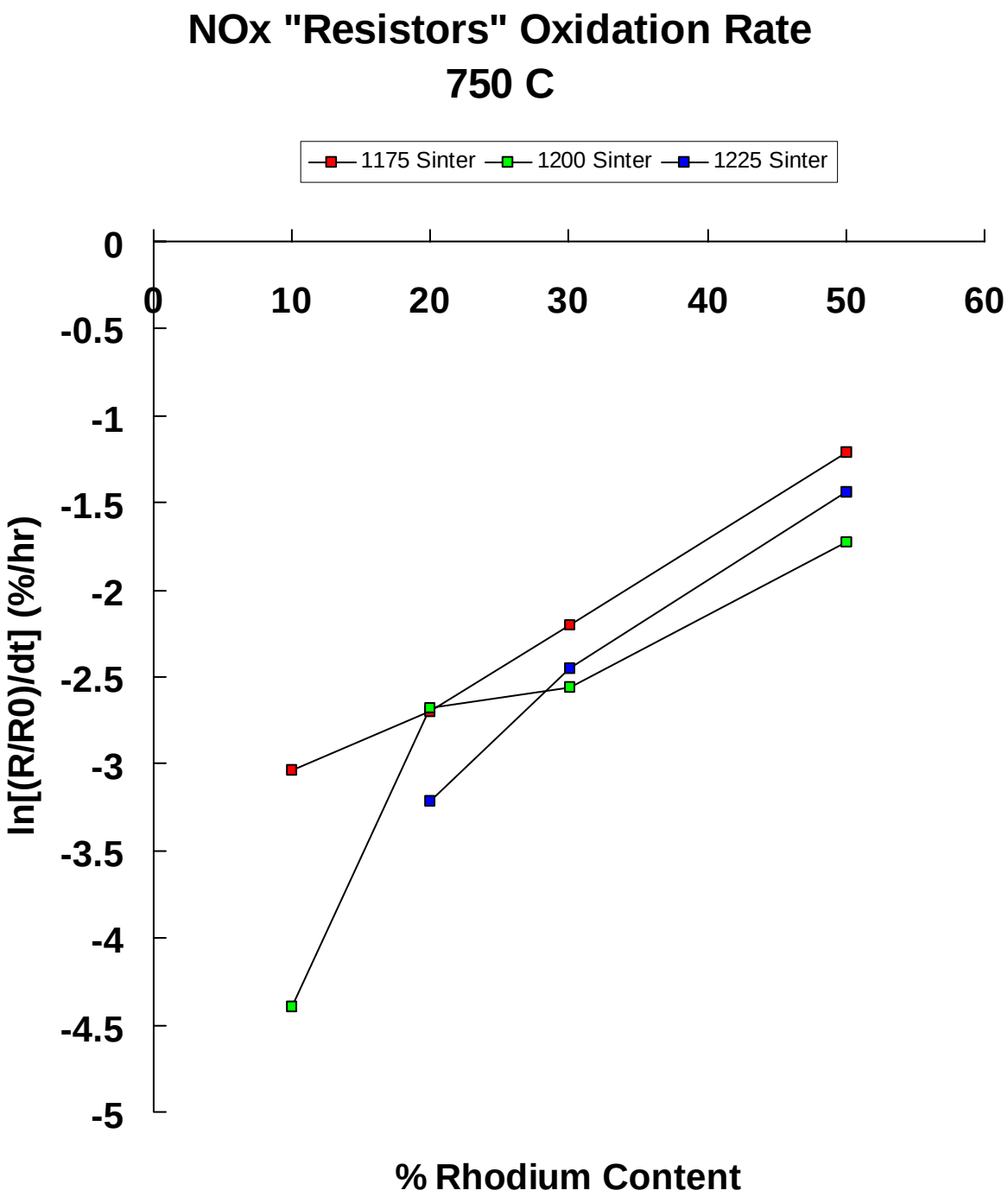
NOx "Resistors" Oxidation Rate
750 C
1175 Sinter
1200 Sinter
1225 Sinter
0
-0.5
-1
-1.5
-2
-2.5
-3
-3.5
-4
-4.5
-5
0
10
20
30
40
50
60
ln[(R/R0)/dt] (%/hr)
% Rhodium Content

Figure IV-8

For 50%/50% Rh/Pt electrodes at 600 °C, the equivalent time is about 7.5 years. From Fig. IV-7 the 10%/90% Rh/Pt electrodes oxidize at least a factor of 7 times slower than the 50%/50% Rh/Pt electrodes. Thus the 10%/90% electrodes would take over 50 years to have a 100% change in resistance.

In reality, the oxidation rates would be even slower than this. First, the tests were done in air, whereas the sensors would be operating most of the time in atmospheres of a few ppm of oxygen. Second, as discussed above, it is possible that the usual operating temperature of about 650 °C combined with the low oxygen content are actually reducing conditions for the 10%/90% electrodes.

Clearly, from a standpoint of oxidation, the 10%/90% Rh/Pt electrode is preferred. However it must be shown that this electrode retains good NO_x sensitivity. In the CeramPhysics test system, a 500 ppm NO_x in N_2 tank is used to supply gas to the test chamber. This gas can be mixed with pure N_2 to get a range of NO_x concentrations between 0 and 500 ppm. It is therefore a convenient metric to specify the sensitivity as the change in sensor current between 0 and 500 ppm of NO_x and this will be used below.

From Phase I of the program, a good sensitivity for the 50%/50% Rh/Pt electrode sensors was a change in current of 220 μA (0 to 500 ppm NO_x) for sensors with three active layers. While it would seem straightforward to test each type of sensor (a matrix of Rh/Pt ratio and sintering temperatures), in practice this is not so easy. Typically the sensitivity decreases the first few temperature cycles until it reaches a plateau (the reasons for this are discussed further in the next section). It would be prohibitively costly in time to take each sensor of the matrix thru the repetitive temperature cycles required.

Therefore a compromise procedure was adopted. Each sensor of the matrix was tested, with a rough gauge of sensitivity being the virgin sensitivity. Tests with one or two of the sensors with the same Rh/Pt ratio were repeated a couple of times to look for trends.

In all cases the sensitivity of the sensors with rhodium contents less than 50% were at least as good as the sensors with 50% rhodium electrodes. This was also true of the last group received and tested, those with 10%/90% Rh/Pt electrodes. Since this group is preferred because it has the minimum oxidation, it was selected for further tests.

Following the sensitivity test procedure outlined above, Fig. IV-9 shows the change in current for a sensor with 10%/90% Rh/Pt electrodes sintered at 1200 °C. The test number refers to a complete temperature cycle from room temperature to operating temperature. In each cycle, the sensitivity was tested at 0.5, 0.6, and 0.7 volts and at temperatures of 700, 750, and 800 °C. In each case, increasing the applied voltage and/or the temperature increased the NO_x sensitivity. The sensitivities in Fig. IV-9 are for the most sensitive case, 0.7 V and 800 °C.

Comparing the sensitivity of this sensor to the sensitivity of the 50%/50% Rh/Pt sensors from Phase I, the result is surprising. It was fully expected that the NO_x sensitivity would drop as the rhodium content of the electrodes dropped. However, the sensitivity for the 10%/90% electrode sensors is about twice the best sensitivity in Phase I. Thus the sensitivity of electrodes with less rhodium was not only as good as the pure rhodium electrodes, the sensitivity appears to increase as the amount of rhodium decreased.

Moreover, as the program progressed, the sensitivity improved by about a factor of three over and above that shown in Fig. IV-9. This latter increase is due to recognizing and correcting the major source of the drop in sensitivity shown in Fig. IV-9. This work is described in the next section.

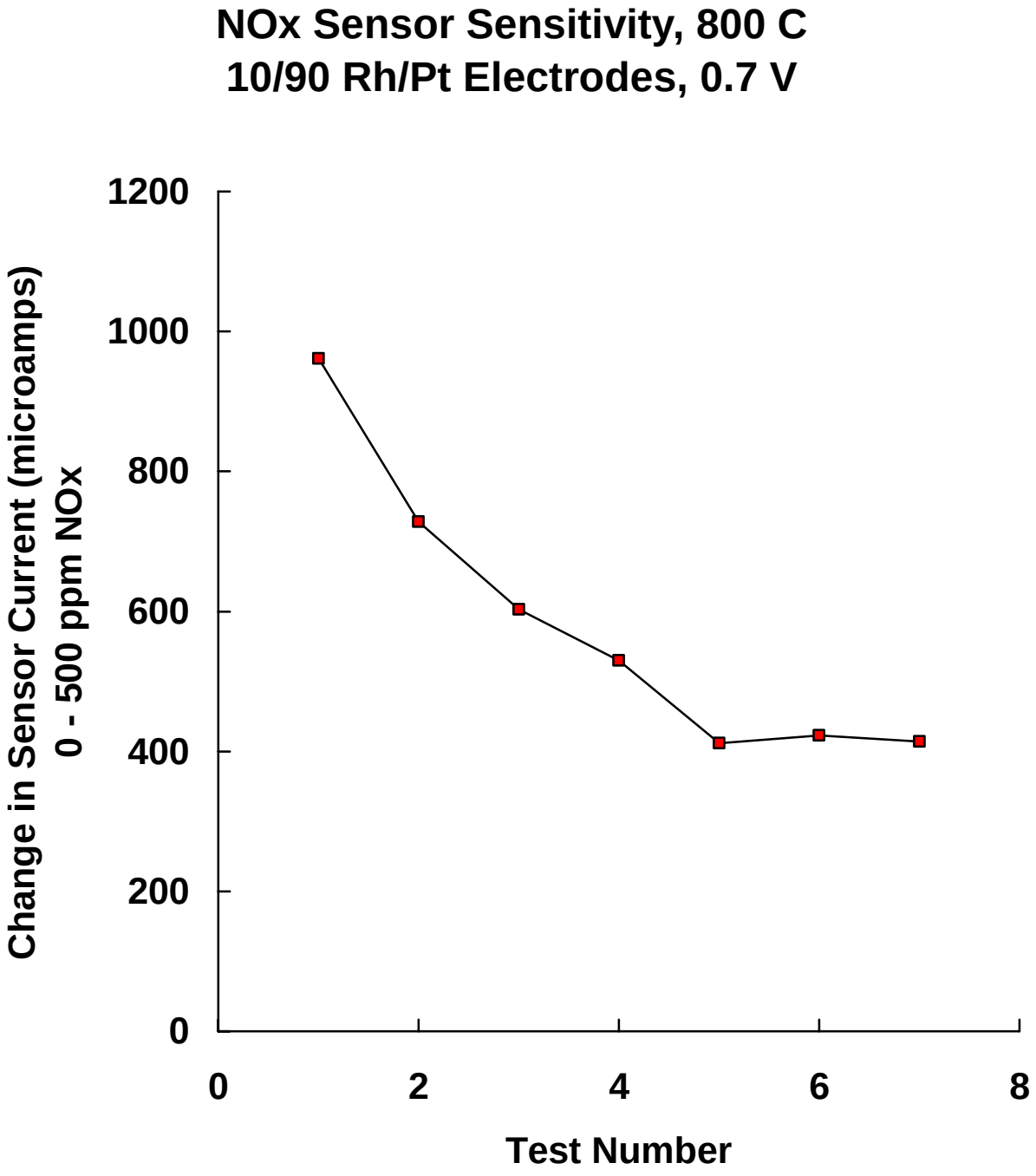
NOx Sensor Sensitivity, 800 C
10/90 Rh/Pt Electrodes, 0.7 V
Change in Sensor Current (microamps)
0 - 500 ppm NOx
1200
1000
800
600
400
200
0
0
2
4
6
8
Test Number

Figure IV-9

Sensitivity Degradation Problem and Resolution

Each of the sensors tested in Phase I and in the sensor evaluation trials of Phase II degraded when repeatably cycled from room temperature to the operating temperature. That is, the maximum current at 500 ppm NO_x and the sensitivity dropped. The rate of degradation varied but was always noticeable after 5-6 cycles and was typically a sizable fraction of the total signal. Sometimes sensors appeared to reach a plateau for several cycles, but then continued to degrade after additional cycles. This is unacceptable behavior and needed to be eliminated.

The source of the degradation has been shown to be increased resistance in the bonds between external leads and the sensor electrodes. These bonds require first a good electrical interdiffusion between the metallic pastes used to fire leads to the bodies and the sensor body internal electrodes. The electrical bonds must also be mechanically well-bonded to the zirconia sensor bodies to prevent mechanical flexing between the leads and the sensor body due to the differential thermal contraction or other stresses that are always present.

Not long after the start of Phase II, this problem was discussed thoroughly with the engineers at MRA Laboratories. This led to testing of alternative methods of attaching the leads while judging results with cross-sectional SEM's of the electrode/lead interface. An expert at Rosemount also examined the data and the SEM's and agreed the problem was likely in the joints.

After multiple variations of attaching the leads, an attachment method was established. The improved attachment method consisted of starting with two light coats of fritted Pt paste (Engelhard A4731) fired on the sensor body electrodes, followed by a thin coat of fritted Au paste (Engelhard A 3338) and finally a thick coat of A3338 to attach the lead to the underlayers. At first, this method seemed to improve (that is, decrease) the degradation, but as more and more tests were done, it was clear that the problem was not yet solved.

To further evaluate the problem, some sensor bodies that had shown degradation were sent to MRA for evaluation. SEM's of one of these sensors are shown in Figs. IV-10 and IV-11. Figure IV-10 shows a cross-section of the sensor body and the bonding pastes (on the right) at 100x magnification. The thin layer (Pt) next to the sensor body is separated by a gap from the thick layer (Au) to its right. Figure IV-11 is even more revealing. This is a 500x magnification of one of the electrodes from Fig. IV-10. Here it is seen that there is also a thin gap between the thin layer of Pt and the sensor body. MRA considers this gap to be the more important in causing the degradation because ideally there should be a good mechanical bond between the frit in the Pt paste and the sensor body.

Finally, MRA pointed out that there is not good interdiffusion between the sensor electrode and the Pt in the paste. The electrode paste appears "speckled" and should be much more diffused into the thin Pt layer.

These SEM's were also shown to a sensor expert at Rosemount and he agreed that poor bonding is the likely source of the degradation. Furthermore, he suggested that the gaps seen in both SEM's may be due to incomplete organic burnout from the pastes during firing.

A possible additional source of degradation might be due to physical changes at the interface between the internal electrodes and the sensor body. However, there are two reasons to reject this theory. First, in Fig. IV-11, there is no visual evidence to suggest any internal changes at this interface. A more powerful argument is provided by a capacitance measurement of the sensor. MRA always measures the capacitance of sensor bodies at 1 MHz after sintering and the

MRA LABORATORIES, INC.
Image Report for CeramPhysics (CS-06-42)
LT-2085, Fired at 1175°C
Friday, September 15, 2006

File: C:\Documen...m Physics (M4-082R)\CS-06-42 (LT-2085, 1175C)\100X.tif
Collected: September 15, 2006 16:32:34

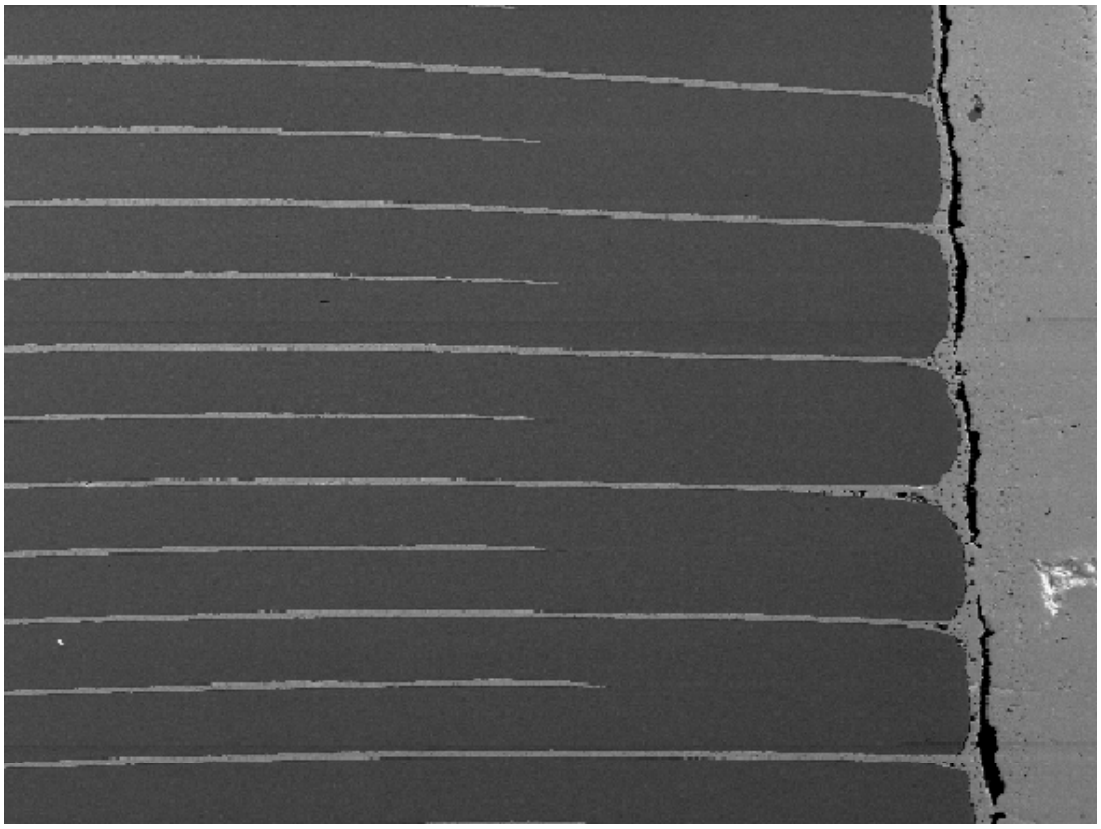

Polished Section at 100X Magnification

Figure IV-10

MRA LABORATORIES, INC.
Image Report for CeramPhysics (CS-06-42)
LT-2085, Fired at 1175°C
Friday, September 15, 2006

File: C:\Documen...m Physics (M4-082R)\CS-06-42 (LT-2085, 1175C)\500X.tif
Collected: September 15, 2006 16:23:33

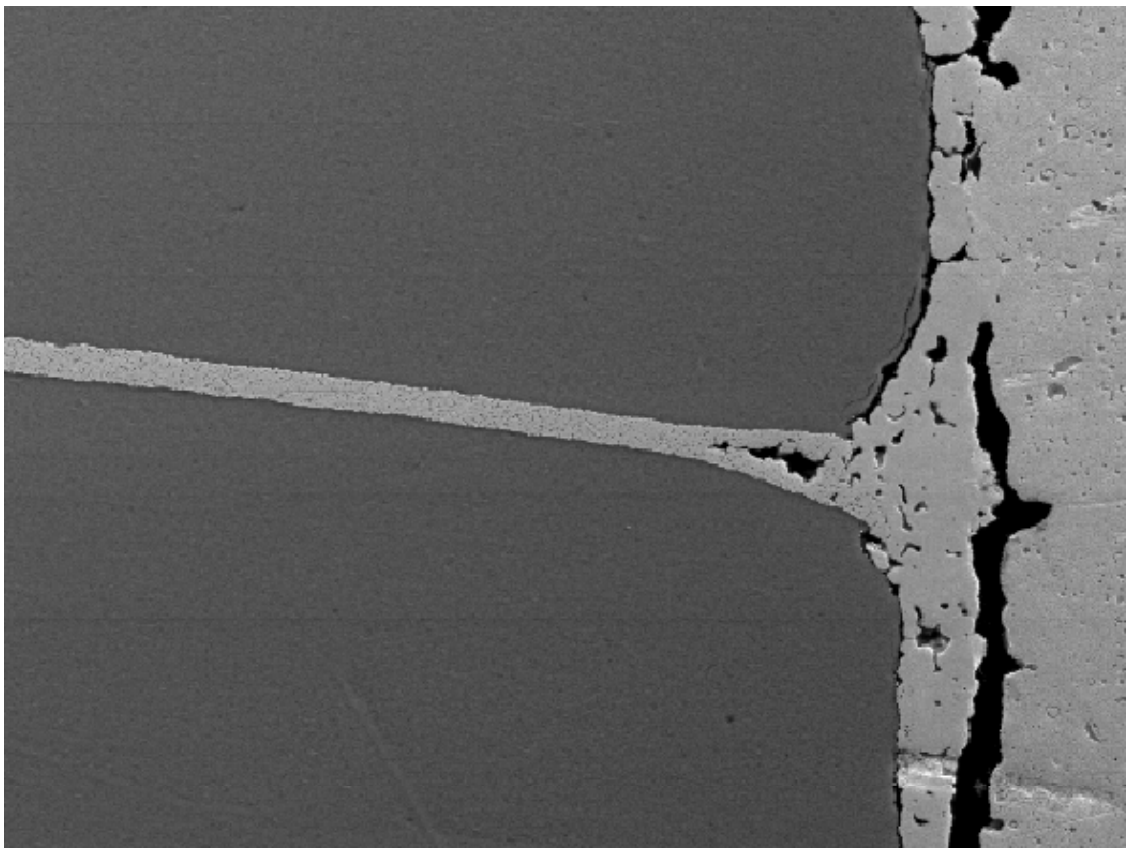

Polished Section at 500X Magnification

Figure IV-11

values are always tightly grouped. The sensor body in Figs. IV-10 and IV-11 had shown significant NO_x sensitivity degradation, but its capacitance had not changed, indicating there are no problems with the internal interfaces.

Assuming that poor bonding in the external joint is the source of the degradation, there are two cures. First, at the suggestion of Rosemount, the firing schedule for the bonding pastes has been significantly altered. The heating rates have been slowed by a factor of 10 or more and there is now a hold at 250 °C to make sure all organics have been removed from the pastes. Second, there is a longer hold at the maximum temperature to ensure better metallic interdiffusion.

This new lead attachment method works as shown in Figs. IV-12 and IV-13. At the suggestion of MRA, the procedure for testing the bond was modified. Instead of relying on the NO_x sensitivity to determine if there was degradation in the contacts, a more sensitive test would be to measure the resistance of the electrodes directly. Therefore, one side of the sensor was ground down to reveal all the electrodes (as in the oxidation tests). Thus electrical contact could be made through the sensor and the resistance of the contact could be monitored and would be a direct measure of the quality of the contact and bonding methods.

The results of a test are shown in Fig. IV-12. Here the sensor was cycled between about 815 °C and room temperature. There is a small increase over the first few cycles, but then the resistance remains very constant up to the end of the tests at 18 cycles.

This test gave confidence that the contacts had been improved, but the real test comes with measuring the NO_x sensitivity. A sensor with 30 layers and sintered at 1150 °C was prepared using the improved lead attachment method and was then tested as a NO_x sensor. The results are shown in Fig. IV-13. The results mirror those in Fig. IV-12 where a small rise in resistance at the start is equivalent to a small drop in sensitivity. In Fig. IV-13, after the initial drop the sensitivity is constant. The results shown in these two graphs indicate that the contact problem is largely, but not completely, solved.

In production, it will be necessary to improve the lead attachment method further. First the attachment pad on the ends of the sensor should be applied using the same paste and inking methods used to apply the internal electrodes. This should result in a superior, well-bonded interface between the external electrode pads, the interior electrodes, and the ceramic sensor body. Lead attachments to the pad should be either wire-bonded or should consist of a metallic path from the sensor body onto the substrate on which the sensor body is mounted.

Operating Characteristics of the 30-Layer Sensor Body

Once the sensitivity degradation problem was solved, it was possible to optimize the other operating parameters without the complicating factor of changing sensitivity. For instance, as shown in Fig. IV-13, changing the applied operating voltage makes no difference in the sensitivity. Figure IV-14 shows the NO_x sensitivity as a function of temperature for a fixed voltage. There is a definite peak in the sensitivity between 650 and 700 °C. This behavior was consistent for all tests at all applied voltages for the 1150 °C sintered sensor. Finally, Fig. IV-15 shows the dramatic decrease in sensitivity with increasing sintering temperature. This decrease occurs because at higher sintering temperatures, there is less electrode porosity and the gas diffusing into the sensor is decreased.

Thus the final physical and operating parameters of the sensor are:

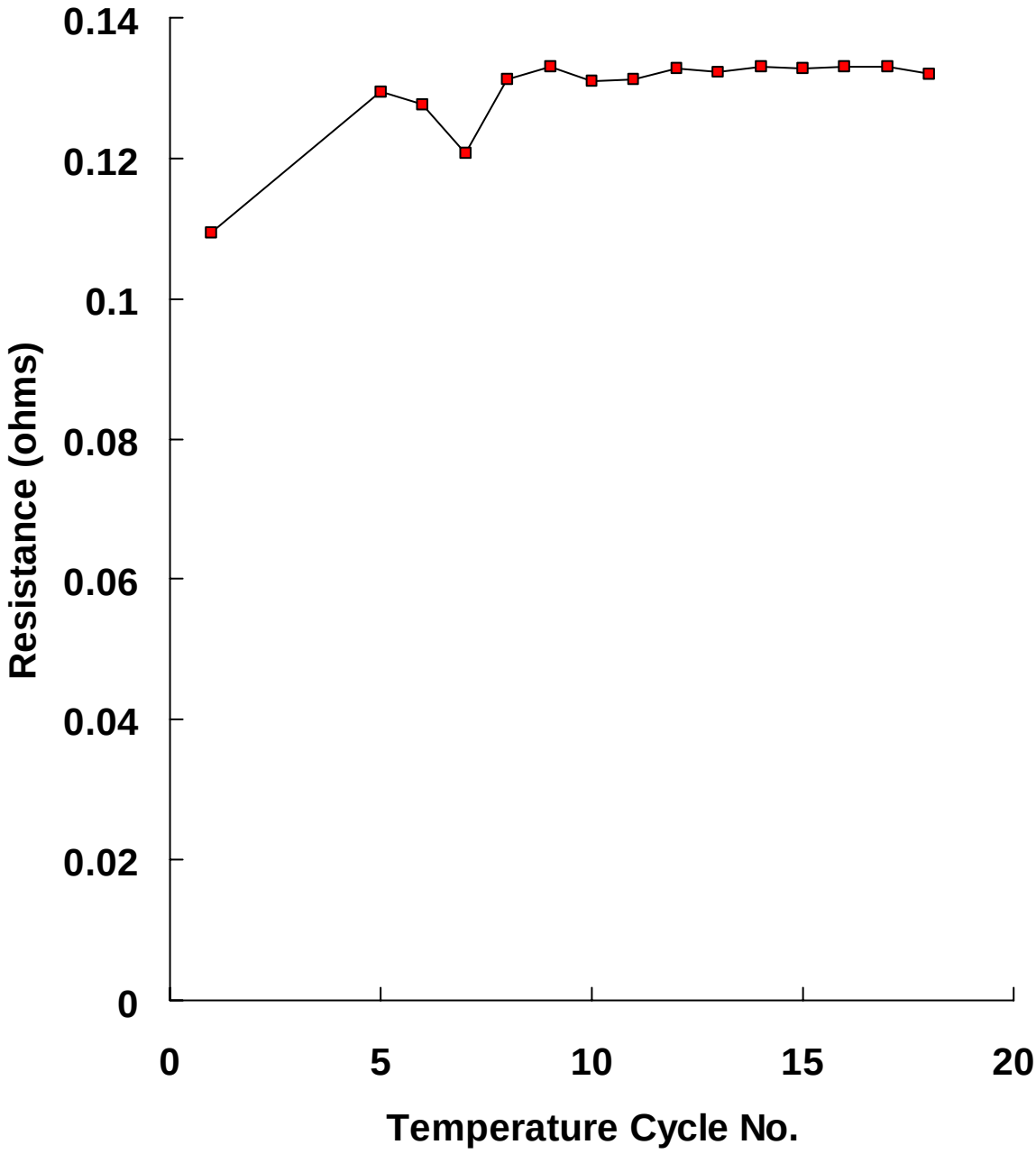
NOx Resistor, Modified
Lead Attachment,
Resistance at 815 C
0.14
0.12
0.1
0.08
0.06
0.04
0.02
0
Resistance (ohms)
0
5
10
15
20
Temperature Cycle No.

Figure IV-12

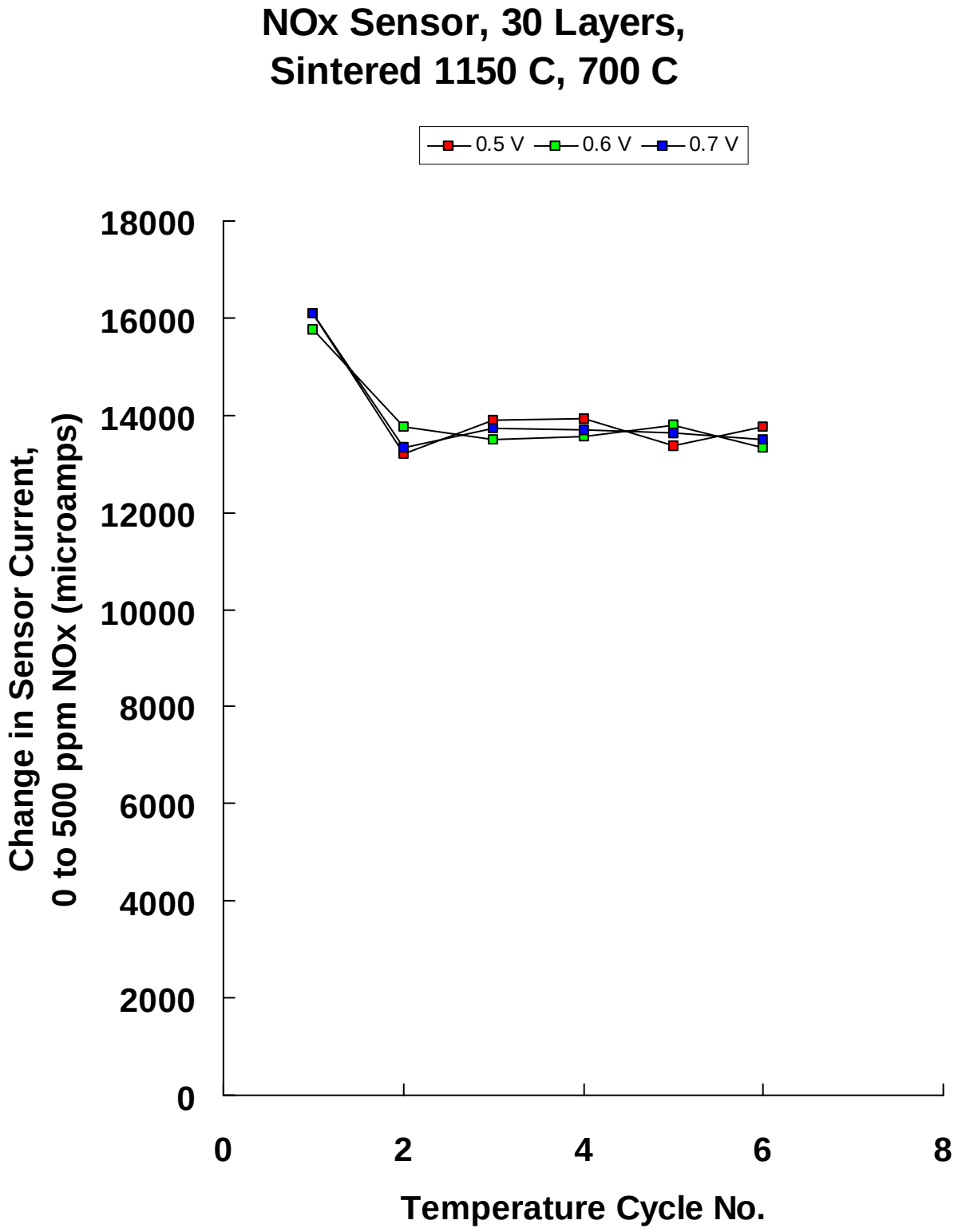
NOx Sensor, 30 Layers,
Sintered 1150 C, 700 C
0.5 V
0.6 V
0.7 V
Change in Sensor Current,
0 to 500 ppm NOx (microamps)
18000
16000
14000
12000
10000
8000
6000
4000
2000
0
0
2
4
6
8
Temperature Cycle No.

Figure IV-13

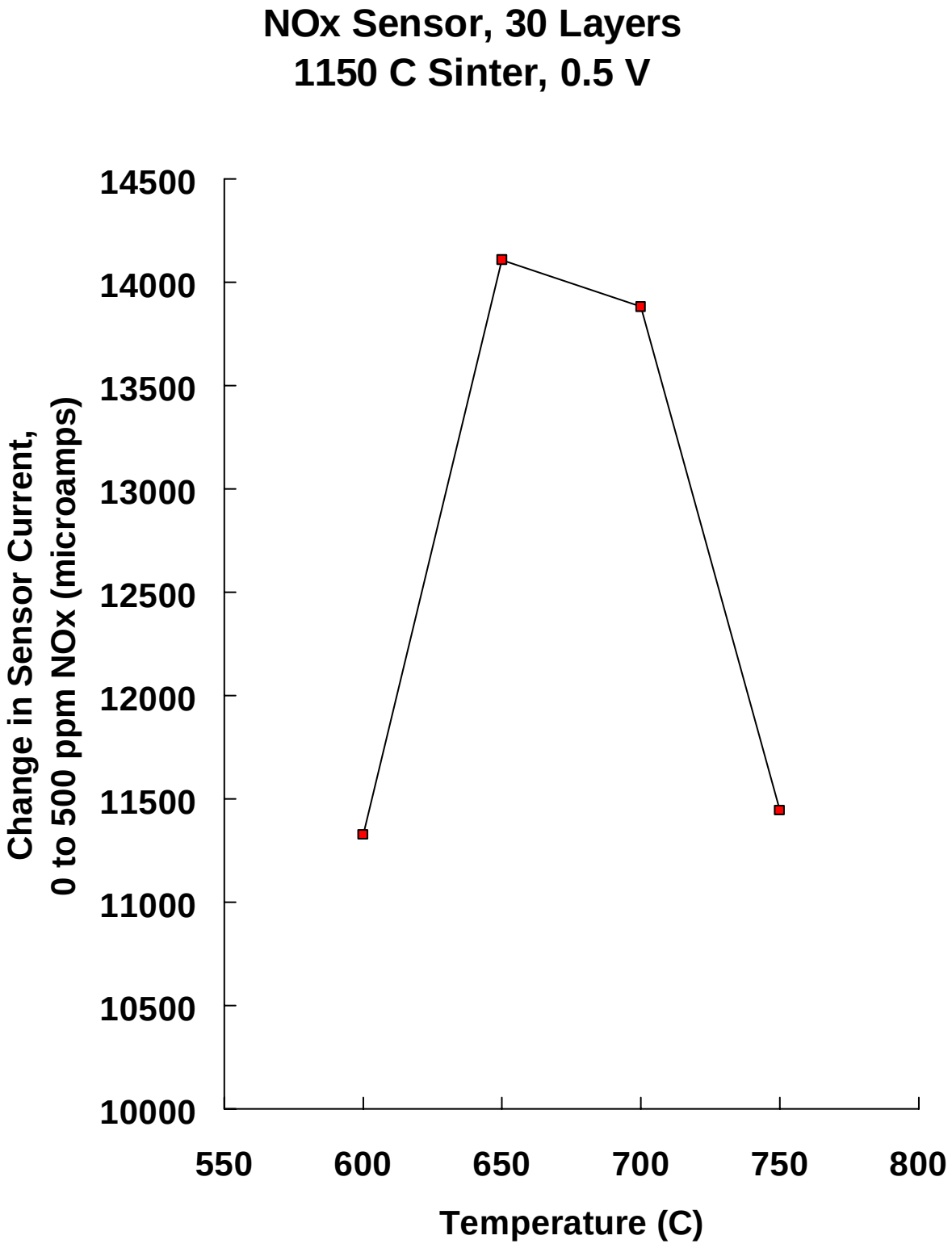
NOx Sensor, 30 Layers
1150 C Sinter, 0.5 V
Change in Sensor Current,
0 to 500 ppm NOx (microamps)
14500
14000
13500
13000
12500
12000
11500
11000
10500
10000
550
600
650
700
750
800
Temperature (C)

Figure IV-14

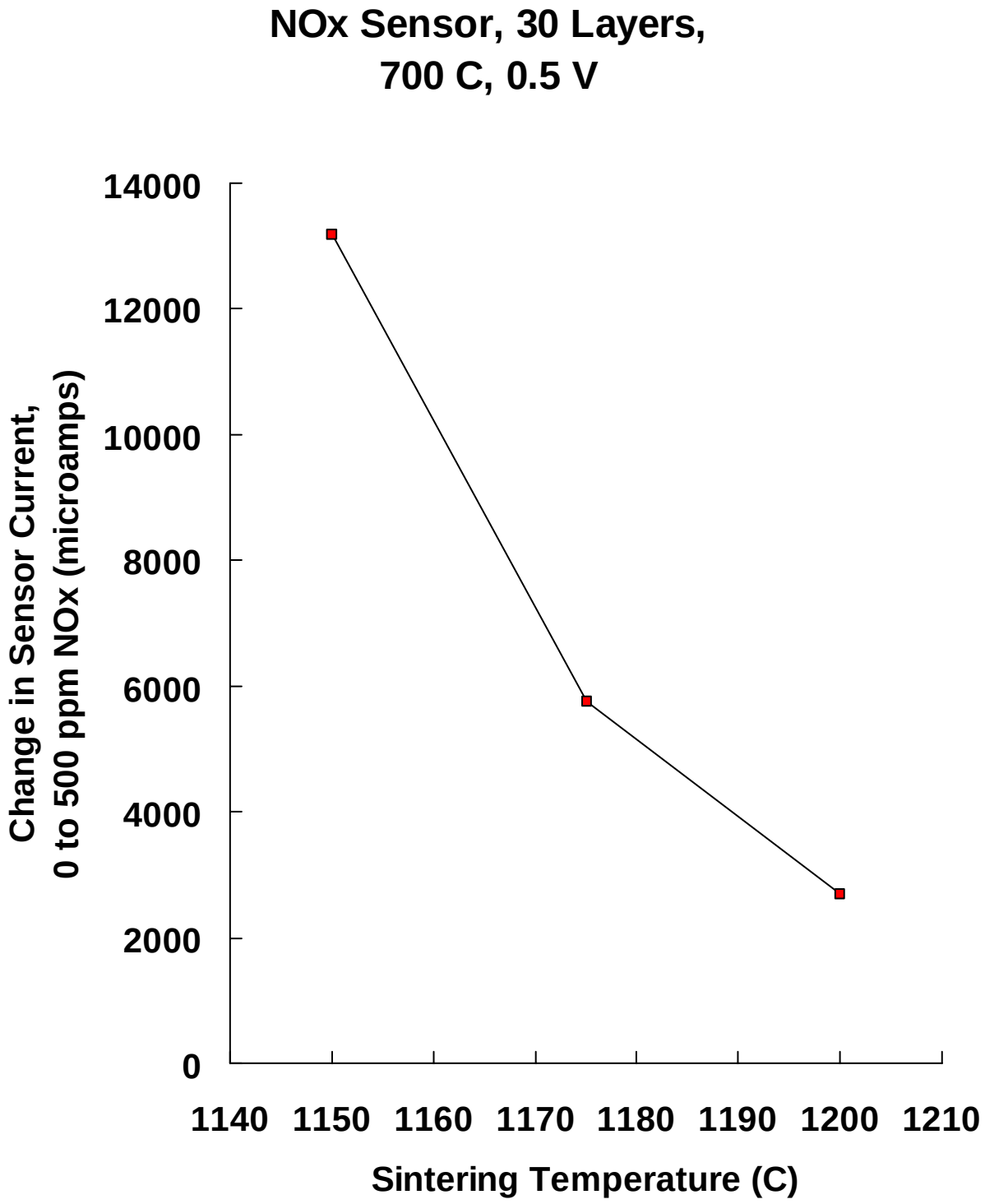
NOx Sensor, 30 Layers,
700 C, 0.5 V
Change in Sensor Current,
0 to 500 ppm NOx (microamps)
14000
12000
10000
8000
6000
4000
2000
0
1140
1150
1160
1170
1180
1190
1200
1210
Sintering Temperature (C)

Figure IV-15

Material	8% yttria-stabilized zirconia
Physical size:	0.177" (L) x 0.164" (W) x 0.123" (H)
Layer Dimensions	0.151" (L) x 0.125" (W) x 0.0031" (t)
Number of layers	30
Sintering Temp.	1150 °C
Operating Temp.	650 - 700 °C
Operating Voltage	0.5 V

There are a number of additional response curves that could be measured at CeramPhysics and these are shown below. Figures IV-16 and IV-17 show the measured sensitivity of a sensor from 0 to 500 ppm NO_x (Fig. IV-16) and 0 to 20 ppm NO_x (Fig. IV-17). Figure IV-16 also shows a fitted linear curve to the data with its equation and correlation coefficient. Figure IV-17 shows a fitted second order curve to the data with its equation and correlation coefficient. These data were measured by mixing gas from a tank of 500 ppm NO_x in N_2 (or 20 ppm NO_x in N_2) with pure N_2 using the measuring equipment described in the equipment description section above. Over most of the range the response is linear at about 28 μA/ppm NO_x. There seems to be a departure from this linearity at low ppm of NO_x as shown in both Figs. IV-16 and IV-17 (there were two different sets of data for the two graphs).

With the equipment available, there were limits on the accuracy of these sensitivity measurements. There was noise in the output of the flow controllers that account for the departures from linearity in Fig. IV-16. There was no way to reduce the noise in the output controllers. It is not clear if the curvature shown in Fig. IV-17 is somehow related to the same noise, is due to some other unrecognized systematic error, or is real.

In any case, the important point is that the sensitivity is very large compared to other amperometric NO_x sensors currently on the market. For instance the commercial NO_x sensor sold by NGK has a typical sensitivity of about 5 nanoamps/ppm NO_x (1).

It has been noted above that the sensor repeats very well upon temperature cycling as long as there is good mechanical and electrical bonding between the external leads and the sensor body. Tests in Fig. IV-18 show the results of multiple cycles between 0 and 500 ppm NO_x while holding the temperature and voltage constant. These data show the sensor behaves as expected with excellent repetition from cycle-to-cycle.

A number of other tests were planned but were not able to be carried out. These include in particular the cross-sensitivity to other gases that are typically present in exhaust gases. CeramPhysics does not have the equipment to make these tests and the costs to purchase the equipment were beyond the resources available in this program. It was planned that these tests would be done by outside institutions. Rosemount had initially agreed to make some of the tests, but have indicated that they do not have an interest in making the sensors commercially and thus have no interest in making these additional measurement. Moreover, even if Rosemount had been willing, they wanted to use the fully-assembled sensors. For the reasons described below, these never became available.

Sensata, Inc. was on a path to test the sensor bodies in many of the desirable tests and had worked on their own packaging for the fully-assembled sensors. However, the group within Sensata that was working on development of the sensor was told by their management to stop work on all NO_x sensors because of the recent turn-down in the automobile industry. As of the

time of submission of this report, Ceramatec, of Salt Lake City, has expressed an interest in testing the sensors and other possible manufacturing partners are being sought.

1. Nobuhide Kato, Yasuhiko Hamada, and Hiroshi Kurachi, "Performance of Thick Film NO_x Sensor on Diesel and Gasoline Engines", SAE Technical Paper Series, 970858, 1997. (Reprinted from Electronic Engine Controls 1997, SP-1236).

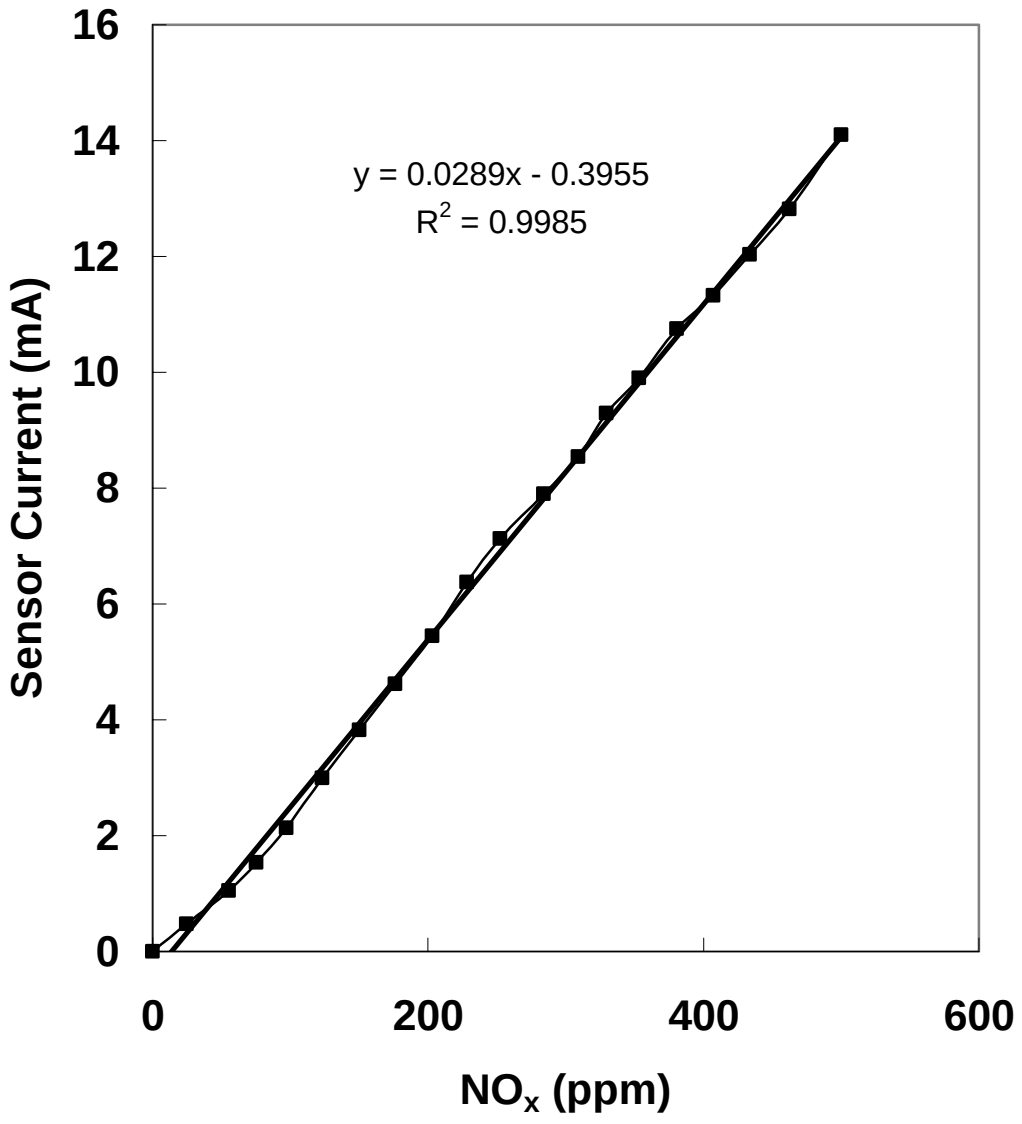
NOx Sensor Calibration
LT-2085, 1150 C Sinter
650 C, 0.500 V
y = 0.0289x - 0.3955
R2 = 0.9985
Sensor Current (mA)
NOx (ppm)
0
2
4
6
8
10
12
14
16
0
200
400
600

Figure IV-16

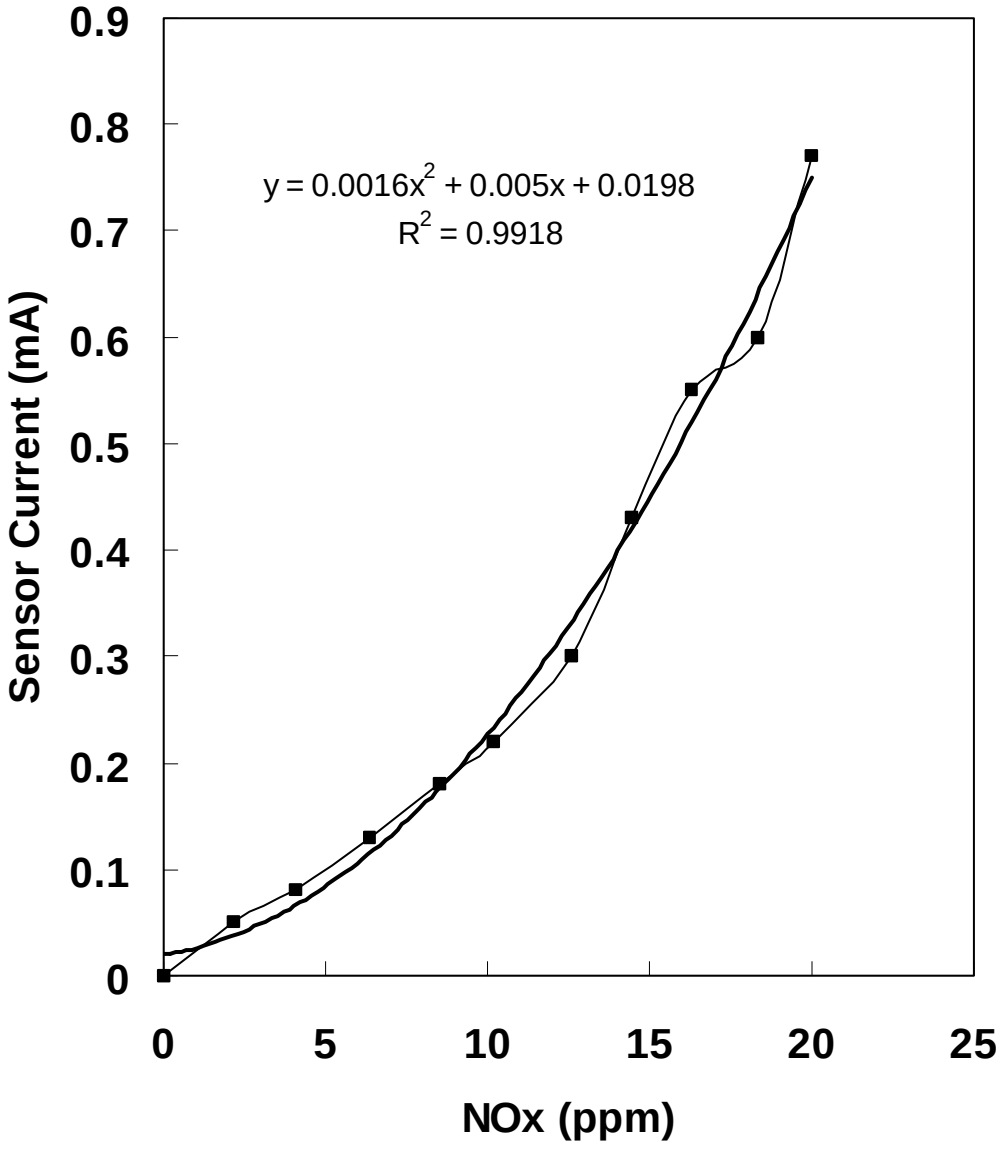
NOx Sensor Calibration
LT-2085, 1150 C Sinter
650 C, 0.500 V
y = 0.0016x2 + 0.005x + 0.0198
R2 = 0.9918
Sensor Current (mA)
NOx (ppm)
0
0.1
0.2
0.3
0.4
0.5
0.6
0.7
0.8
0.9
0
5
10
15
20
25

Figure IV-17

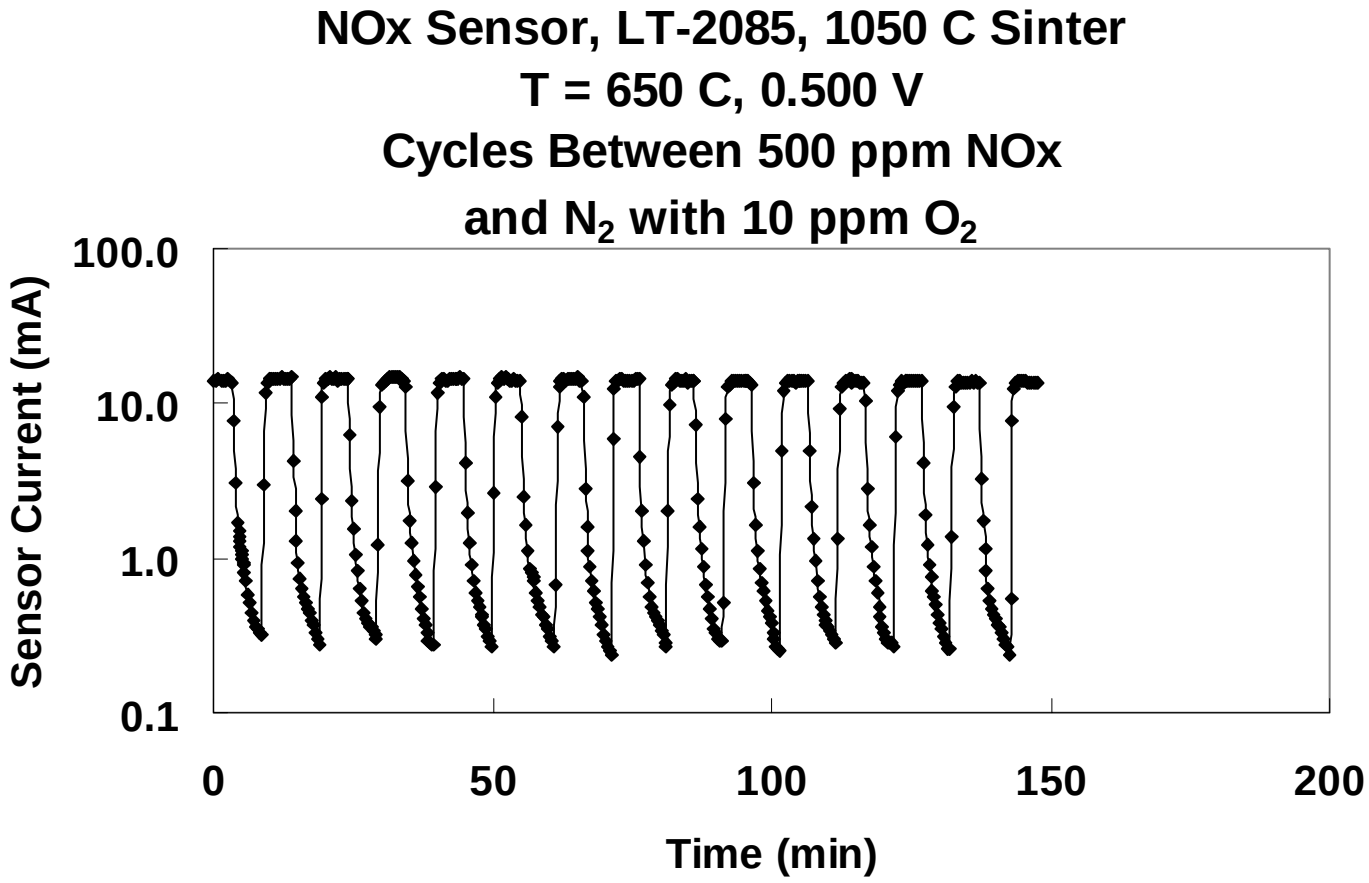
NOx Sensor, LT-2085, 1050 C Sinter
T = 650 C, 0.500 V
Cycles Between 500 ppm NOx
and N2 with 10 ppm O2
Sensor Current (mA)
100.0
10.0
1.0
0.1
0
50
100
150
200
Time (min)

Figure IV-18

V. FULLY-ASSEMBLED SENSOR: PROBLEMS, SUCCESSES, FUTURE DEVELOPMENT

Overview and Review

The rhodium used in the electrode of the NO_x sensor catalyzes both NO_x and oxygen. Therefore the oxygen must be separately detected with a dedicated oxygen sensor and this signal must be subtracted from the total signal from the NO_x sensor body to obtain an accurate measurement of the NO_x only. A typical exhaust gas might consist of 2-3% O_2 (20,000 - 30,000 ppm) while the NO_x content might be 10 - 100 ppm. In order for the NO_x signal not to be overwhelmed by the O_2 signal, it is necessary to find a method of lowering the O_2 content of the gas. The same problem is common to all amperometric NO_x sensors.

The preferred oxygen sensor is a miniature multilayer zirconia sensor developed in the companion DOE oxygen sensor program. The only difference between this oxygen sensor and the NO_x sensor is the electrode material. In the oxygen sensor, the electrode is made of platinum or a platinum-gold alloy. This electrode does not catalyze and detect NO_x, only oxygen.

In the original conception (described in detail in the next section), the gas to be measured would pass thru a diffusion-limited porous plug into a small chamber or shell with walls made of yttria-stabilized zirconia (YSZ). Electrodes on the inner and outer surfaces of the shell would be used to remove most of the oxygen from the chamber through the walls of the shell (see below). The NO_x and O_2 sensor bodies would be inside this shell, and the entire assembly is designated as the "**fully-assembled sensor**". The shell would also be attached to a manifold to insert the sensor into the exhaust gas (similar to the manifold of a commercial auto oxygen sensor). Leads would enter the interior of the shell thru a feed-thru plug at the opposite end of the shell from the porous plug. The active section of the entire shell would be heated to the sensor operating temperature (e.g. 650 °C). Since YSZ is a poor thermal conductor, the shell can be long enough so that the manifolded end of the shell is at the wall temperature of the manifold. An approximate scale drawing of the original design of the shell and the plugs is shown in Figs. V-1 and V-2. Later in the program, the shell was shortened, but all other features were maintained.

The oxygen can be removed from the interior of the shell because the shell is made from an oxygen conducting material, 8% yttria-stabilized zirconia. Applying a voltage of the correct polarity between the electrodes on the inside and outside of the shell (the "pumping surface") will catalyze oxygen into oxygen ions on the interior surface, transport the ions through the shell to the outer surface where they will recombine into oxygen molecules.

In order to design the shell, several constraints needed to be taken into consideration. First, the response time of the sensor depends on the pumping speed for removal of oxygen from the interior, and it is desirable to minimize this response time. Second, the mass of the shell must be minimized to minimize the heat-up time of the sensor. Third, the shell and plug must be manufacturable.

Originally, the zirconia shells were to be made by Zircoa and the porous plugs by Filtros. Early in the second phase of the program, Filtros sent some sample plugs with three different porosities, although they did not provide any data describing pore size, % porosity, etc. After that they did not respond to further inquiries. Zircoa never did deliver any zirconia shells. They promised them month-after-month, but were not able to make them. Finally, MetaMateria

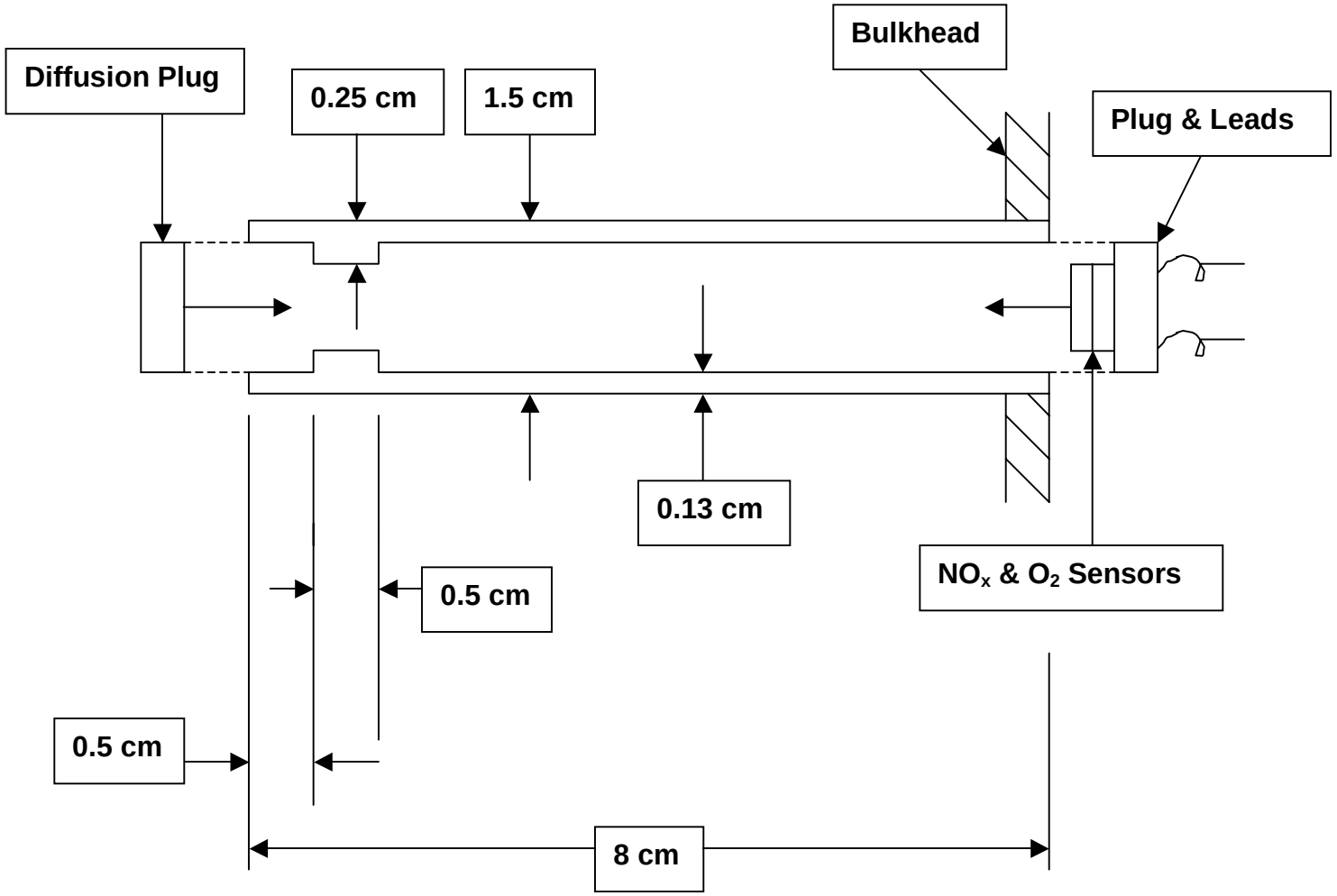
Diffusion Plug
0.25 cm
1.5 cm
Bulkhead
Plug & Leads
0.13 cm
0.5 cm
NOx & O2 Sensors
0.5 cm
8 cm

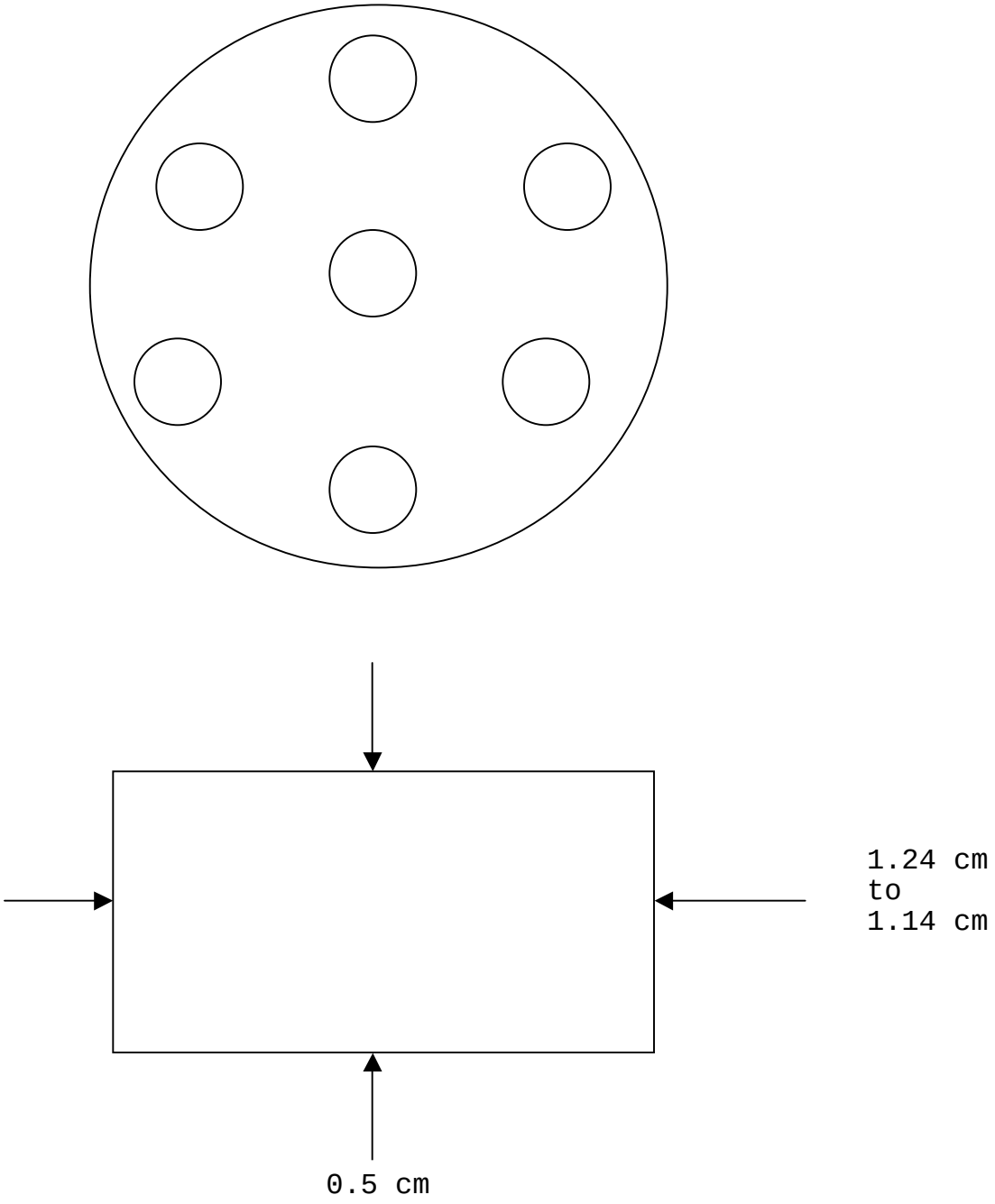

Figure V-2

Partners of Columbus, OH was contracted to make both the shells and the diffusion plugs. In order to assure that some shells could be made, the overall length was reduced to 5 cm.

Detailed Description of the Fully-Assembled Sensor

A detailed description of the design considerations for the fully-assembled sensor is given below. There are some rather mundane, but important additional considerations. The plugs must be bonded into the shell and lead holes around the lead wires must be sealed, an appropriate heating method needed to be developed, an appropriate feedthru at the cold end of the shell needed to be identified, and an external lead connection scheme needed to be developed. The solutions to these problems are described below.

The basic shape of the sensor shell is shown in Fig. V-1. It consists of a cylindrical tube and two plugs, with all three pieces made of 8% yttria-stabilized zirconia. Two shoulders inside the shell provide an edge against which the two insert plugs will seat. The diffusion plug on the left is porous to allow gas to enter the interior of the shell. The plug on the right has holes for wires to access the interior of the shell and these wires will exit the sensor thru a hermetic seal at the right end of the sensor. The entire assembly shown will be surrounded by the test gas containing oxygen and NO_x. The right end of the tube will be sealed to a bulkhead feedthru to connect the sensor to the outside world. After Zircoa had trouble making the shells, the original length of 8 cm was later reduced to 5 cm to make the shell easier to make.

There are two considerations that drive the design. First, the internal open volume containing the sensor bodies must be as small as possible to minimize the response time, where there is a trade-off between the porosity of the filter open to the test gas and the pumping speed (and current) required to remove excess oxygen from the interior. Second, it is desired to make the mass as small as possible to minimize the heating time and to keep the temperature as uniform as possible. The effects of these requirements on the dimensions are discussed below.

The overall length of the sensor has to accommodate the width of the plugs at each end, a pumping surface platinized inside and out for removing the interior oxygen, and a length of tube sufficient for a thermal standoff between the heated sensor and the unheated feedthru.

To minimize the mass and thus the heating time, the diameter should be as small as possible, the walls should be made as thin as possible and the heated length should be kept as short as possible. A choice will be made for each dimension and the implications of the choices will then be considered in light of the requirements on the sensor. First, the length of each plug will be fixed at 0.5 cm. The width of the platinized pumping surface will be taken as 0.5 cm, and the length of the unheated tube (the thermal standoff) will be taken as 3.5 cm, after the reduction in length discussed above. (The total length of the thinner wall at the right will thus be 4.0 cm.) The length of the inset for the diffusion plug will be 0.5 cm. The wall thickness of each end of the shell will be taken to be 0.13 cm and the wall thickness in the center section will be taken as 0.2 cm. The plugs will be smaller in diameter than the inner diameter of the shell by 0.1 cm, thus leaving an annular gap of 0.05 cm to be filled in with the bonding material. Inside the shell, there will still be an edge 0.07 cm in width for use as a seating surface for the plugs.

The only dimension not selected above is the inside diameter of the open volume. The final NO_x multilayer bodies will have dimensions of 0.45 cm (L) x 0.417 cm (W) x 0.312 cm (H). These multilayers are smaller in area than the oxygen sensors that will be used internally inside the shell, and these have dimensions of 0.65 cm (L) x 0.50 cm (W) x 0.147 cm (H). The internal NO_x

and O_2 sensors can be stacked on each other and bonded to the interior of the solid plug with leads for them exiting through the plug. Thus the interior diameter of the shell must at minimum accommodate the diagonal of the oxygen sensor body, that is, it must be at least 0.82 cm. However, in order not to block the lead exit ports, the inner diameter must be increased to 1.0 cm. The leads going thru the holes will be electrically insulated with short sections of 1/16" single hole mullite tubes available from Omega. The inner diameter must be increased to accommodate these tubes as shown in Fig. V-2 which is a scale drawing of the feed-thru plug.

The implications of these choices are discussed below. First, the wall thickness at the right end is only 0.13 cm, and this must provide mechanical strength to the sensor. For comparison, the 13 cm long zirconia tubes used in the Thermox analyzer have wall thicknesses of 0.13 cm. Thus this same wall thickness should be sufficient for a shorter piece, and this is the reason this dimension was chosen.

Next consider the implications for the heating times. The heater is a resistance wire that will be wrapped around the tube. For uniformity of temperature, the heater wire should be spread as uniformly as possible over the active length of the shell, meaning the 1.5 cm at the left end in the drawing. The zirconia shell is not an electrical conductor, but it is a good ionic conductor. However, the platinized pumping surface is conducting, and for isolation, the heater wire must be electrically isolated from both the shell and pumping surfaces. Therefore it will be necessary to wrap the heater around the shell on the outside of each plug, avoiding the pumping surface.

The volume of the sensor including the shell, plugs and three sensor bodies can now be calculated. It is assumed the heater will cover the shell from the left (open) end to the right edge of the feed-thru plug in Fig. V-1. The unheated mass of the shell extending to the right can be accounted for as follows. There will be a linear gradient in temperature between the heated section of the sensor and the manifolded feedthru at the extreme right end of the tube. Since the specific heat at these temperatures is approximately constant, it is a good approximation to take 1/2 the length of the unheated shell as the appropriate mass in the calculations below. The resulting volume of the shell, plugs and sensors is 4.03 cc. Since the density of zirconia is 5.89 g/cc, the mass to be heated is 23.72 g.

The mass is needed to design the temperature controller to heat the sensor in a reasonable time. For adiabatic heating, the relationship between the heater power and the heating rate is given by:

$$Q = m\,C\,(\Delta T/\Delta t) \qquad \text{(Eq. V-1)}$$

where Q is the power input (W), m is the mass (g), C is the specific heat and ΔT (°C) is the temperature change over time Δt (s). For high temperatures, C is given by the Debye approximation, C = 3nR where n is the number of atoms per unit cell (3 for ZrO2) and R is the gas constant. Therefore C = 74.8 J/mole/K and since there are 123 g/mole in ZrO2, C = 0.608 J/g/K.

The sensor will normally operate in an exhaust gas, which is at some elevated temperature. However, there may be times when the ambient gas is at room temperature. The sensor heater must be capable of heating the sensor from room temperature to the operating temperature (e.g. 750 °C) in a reasonable time for testing purposes within this program. It is desirable to keep the maximum output power from the controller as low as possible, both to reduce the size and cost of the internal transformer and to minimize heat-sinking within the power supply. Therefore, if

possible, the output voltage should be no more than 12 V and the power should be limited to 15 W, that is, to a current no more than 1.25 A.

Choosing a current of 1.2 A at an output voltage of 12 V, or Q = 14.4 W, and a temperature change of (750 - 25 °C) = 725 °C (worst case of 750 °C operating temperature), then the heating time, Δt, can be calculated as 12.1 minutes, which is a reasonable time for testing purposes within this program. Clearly, if the sensor is in a heated exhaust stream, the warm-up time will be shorter.

This analysis leaves room for radiation, conduction, and convection losses. It is hoped that thermal losses can be held to about 5-10% of the total heat output when heating from room temperature. Several different insulations and combinations of insulations were tested during the course of the program. The final configuration of insulation selected was a thin layer of a silicate wool wrapped next to the sensor shell surrounded by light-weight ceramic insulation board made by Thermotect.

Given the voltage and current requirements above, the heater resistance will be 10 ohms. This is a reasonable resistance and can be matched to available heating wire. For instance, Kanthal A-1 wire, 29 gauge, has a resistance of 6.88 ohms per foot. Therefore, a length 1.45 ft long can be wrapped around the sensor body in 7-8 turns, allowing for some free wire at the ends. To anchor the wire thermally to the shell, it will be necessary to use a potting material that is thermal-expansion-matched to the zirconia shell.

The temperature controller will also have a second, independent section designed to control the oxygen content of the interior gas. This section of the controller will read the output of the internal oxygen sensor and control the oxygen content by pumping out oxygen across the 0.5 cm wide band of platinum on the inner and outer surfaces of the sensor.

The power output for this section of the controller must also be specified. That is, what must be the current and voltage output from the controller to keep the interior almost free of oxygen? The answer depends on how fast the gas inside the sensor is replenished through the diffusion plug, and there is a trade-off here. The gas needs to be replaced quickly enough that the internal composition tracks the external composition. But too fast a diffusion rate will require too large a pumping current. Because of these uncertainties, sample diffusion plugs from Filtros with three different diffusion rates were considered. For design purposes, assume the gas inside the sensor will be completely replaced once every 10 sec (however, it is expected that the response to changes in the NO_x content of the exhaust gas will be much less than 10 sec).

The volume of the internal space (subtracting the volume occupied by the sensors) is 0.302 cc. From Faraday's law, a flow of oxygen thru an oxygen conductor of one liter/min requires 287 A. Therefore, if the gas were all oxygen, to completely evacuate the space every 10 sec would require 520 mA. However, in the worst case, the gas in the interior will be air at 20% oxygen content. Therefore the maximum current required will be 104 mA. In most cases, the sensor will be in exhaust gas with even smaller oxygen content, requiring even less current. For design purposes for the controller, it will be assumed that a maximum current of 130 mA will be required. It is hoped that this is a sufficient current to evacuate the open volume while allowing for significant porosity in the porous plug (which is equivalent to fast response time).

This current should be consistent with the maximum voltage of 12 V available from the power supply. The resistance of an oxygen conductor with parallel faces is given by

$$R = (t/A)(T/\sigma_0)\exp(\theta/T) \qquad (2)$$

where t and A are the thickness and area of the oxygen conductor, T is the temperature in Kelvin (assume the worst case of 1023 K = 750 °C), and σ_0 and θ are parameters describing the conductivity of an oxygen conductor. For 8%YSZ, σ_0 = 1.623 E6 K/ohm-cm and θ = 1.1954E4 K. Approximating the tube surface area by using the average diameter of 1.25 cm, the resistance calculated from Eq. 2 is 8.2 ohms. In other words, a current of 0.13 A requires a voltage of 1.06 V, well below the upper limit of the controller.

Lead attachments to the sensors are a separate problem with different (and better) options available for a production sensor than for the test sensors to be made in this program. In production there can be an investment in equipment and materials which is not practical for this program. For instance, in production, wires can be attached to the faces of the NO_x sensor with a spot welder or metal can be applied in a continuous track along a substrate to the sensor. In this program, leads will be attached to the face of the sensors with the same gold paste used previously. As discussed above, these leads will exit the sensor through holes designed into the feed-thru plug of Fig. V-1., where they will be attached to extension leads. A thermocouple will also be potted into a blind hole on the outside of this same plug. Another wire through this plug will be attached to the inner oxygen pumping platinum band.

On the outside of the shell, there will be one wire for the outer oxygen pumping platinum band and two wires for the wire heater. Thus there will be a total of 14 wires exiting from the shell, and these must all be kept electrically isolated from each other.

Electrical connections to leads will be made with the gold paste (fired at 850 °C) used to attach leads in the previous tests of the NO_x sensor, and with crimp joints for the heater wires. The optimum material of the wires used for all these leads required some development work as described below.

With the design as drawn in Fig. V-1 there is one serious problem: there is no way to get the wires attached to the outside of the shell into the interior of the shell so they can exit through the hermetic seal. Also, as noted above, the length of the zirconia shell had been reduced to make the shells easier to make, but it was still desirable to have a longer length of thermal standoff.

To solve these two problems, a stainless steel tube 6" long was slipped into the right end of the zirconia shell in Fig. V-1 and held in place with the Aremco bonding material. Half the diameter of a short section of this tube was removed at this end over about a 1" length, leaving an opening for the outer leads to feed into the interior of the tube.

All leads will exit the end of the tube to the right in Fig. V-1 through a seal of high-temperature RTV silicone material. A flange with a central o-ring seal is slipped over the end of the stainless tube and the leads are attached to home-made multipin connectors.

Assembly of the Full Package, Problems and Solutions

Multiple problems were encountered in the assembly of the full sensor and the assembly of the full sensor turned out to be significantly more demanding than originally thought. Most of the problems were overcome to the extent that at the end of the program a fully-assembled sensor was tested to a limited extent. All the subsystems were shown to work to the extent that the concepts behind the basic design were shown to be valid. However, there were still subsystems that did not work well enough to allow additional testing at outside companies. There were not

enough resources of time or money to continue development. The problems that were encountered, that were overcome, and that remain are discussed below.

These problems have generated ideas about modifications to the packaging of the sensor necessary before the fully-assembled sensor can be put into production. These thoughts were also spurred by the developmental approach taken by Sensata before their management stopped work on all NO_x sensors. The modified approach for the future is discussed below.

After completion of the design of the fully-assembled sensor at the beginning of Phase II of the program (Figs. V-1 and V-2), the zirconia tubes were ordered from Zircoa and diffusion plugs from Filtros. Filtros eventually sent three sets of sample diffusion plugs with three different porosities. However, over a year went by with Zircoa constantly promising to sent the zirconia shells, but without delivering them. In retrospect, the shells were probably too long for the manufacturing method used by Zircoa. As noted above, MetaMateria Partners was eventually contracted to make both the shells and the diffusion plugs.

In the meantime, without the shells, neither the diffusion plugs nor the oxygen controller could be tested and thus there was no learning curve involving the assembly of the sensor. In desperation, alternate methods of testing the diffusion plugs were explored by bonding diffusion plug samples from Filtros to sections of used oxygen sensor tubes made for the Thermox oxygen sensor. These tests highlighted some problems with the controller which were ultimately corrected. The tests indicated that a diffusion plug with a medium porosity would be a good choice and MMP made about 30 plugs with this porosity. (As seen below, plugs with a lower porosity would have been a better choice).

The next problem was finding a good insulating/bonding material for use in the assembly. The material would be used to anchor leads to the sensor bodies, bond the sensors to and seal the feedthru holes in the blocking plug, bond the plugs into the shell, attach the zirconia shell to the stainless steel extension tube, and provide an insulating undercoat and bonding overcoat for the heater. Multiple different high temperature bonding materials were tested. All failed, usually because the material was not thermal-expansion-matched to the zirconia or could not take the high temperatures associated with the sensor.

Finally, an engineer at Aremco offered to formulate a material that would meet the requirements of the program. This is a one component material with about the consistency of Elmer's glue and is fired on a schedule with a peak temperature of 370 °C. The material is zirconia-based, has good insulating properties, and is very well thermal-expansion-matched to zirconia. Its minor drawback is a tendency to sometimes bond weakly to zirconia, especially polished surfaces. However, when it does bond, a significant amount of shear force is required to remove it and it can be thermally cycled multiple times without failure. The material was so close to meeting our needs that within a few months, Aremco added the material to their product list.

After solving the problems above, the methods for assembling the full sensor could be attacked. Figures V-3-6 show various parts of the full sensor in various stages of assembly. Figure V-3 shows all the separate parts to be assembled, starting (left to right) with the diffusion plug, the zirconia shell, the NO_x sensor, the oxygen sensor, the feed-thru plug and the stainless steel extension tube. Figure V-4 shows the platinized oxygen-pumping surface on the outside of the shell. Figure V-5 shows the wrapped heater on the outside of the shell covered with the Aremco bonding material and the pumping surface lead attached with gold paste. There is an unseen underlayer of the bonding material that insulates the heater wire from the shell. Also shown is a bridge of the heater wire across the pumping surface connecting the two sections of the heater.

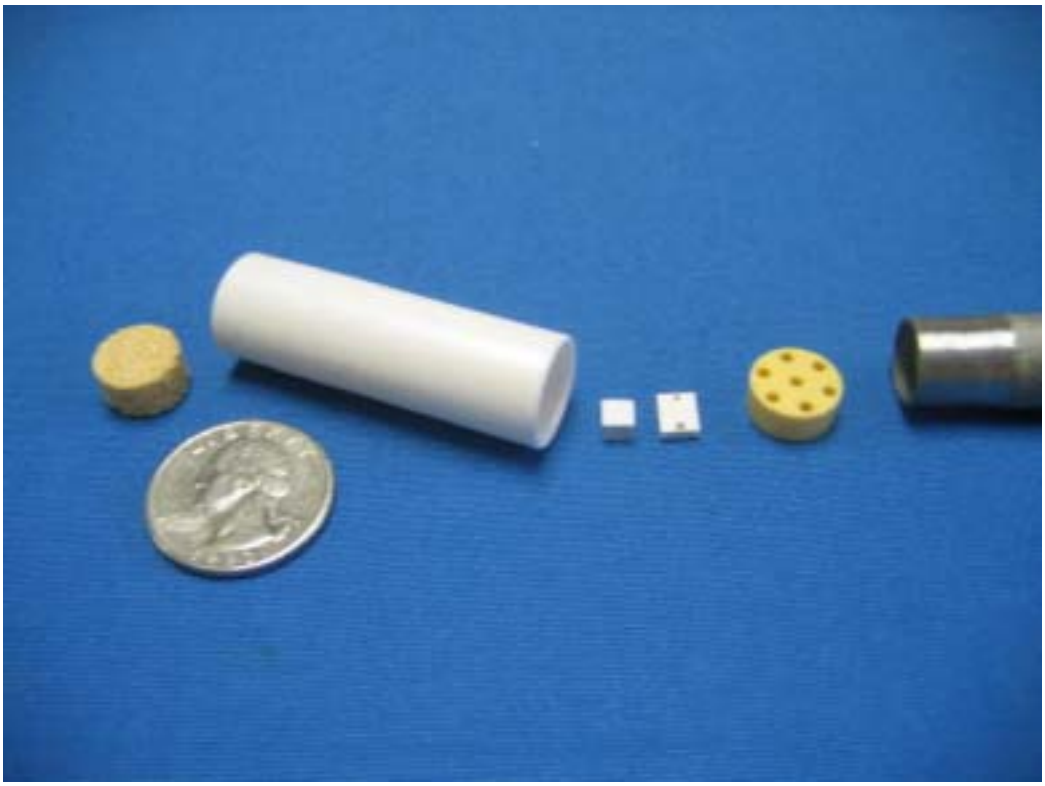

Figure V-3

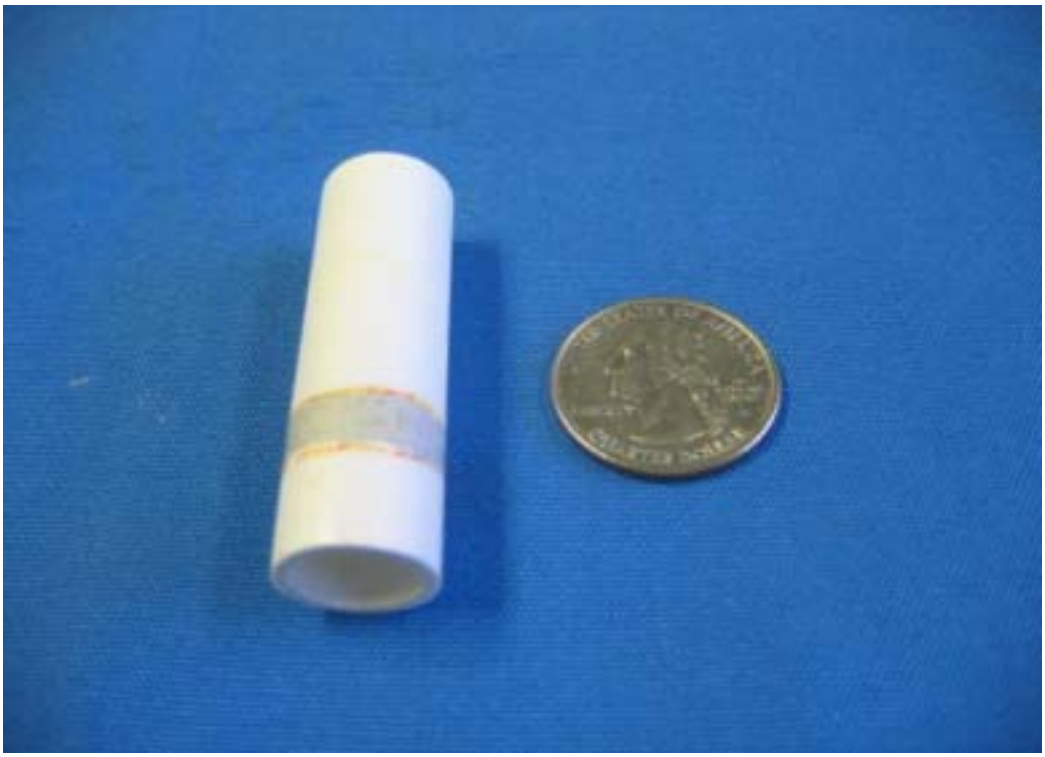

Figure V-4

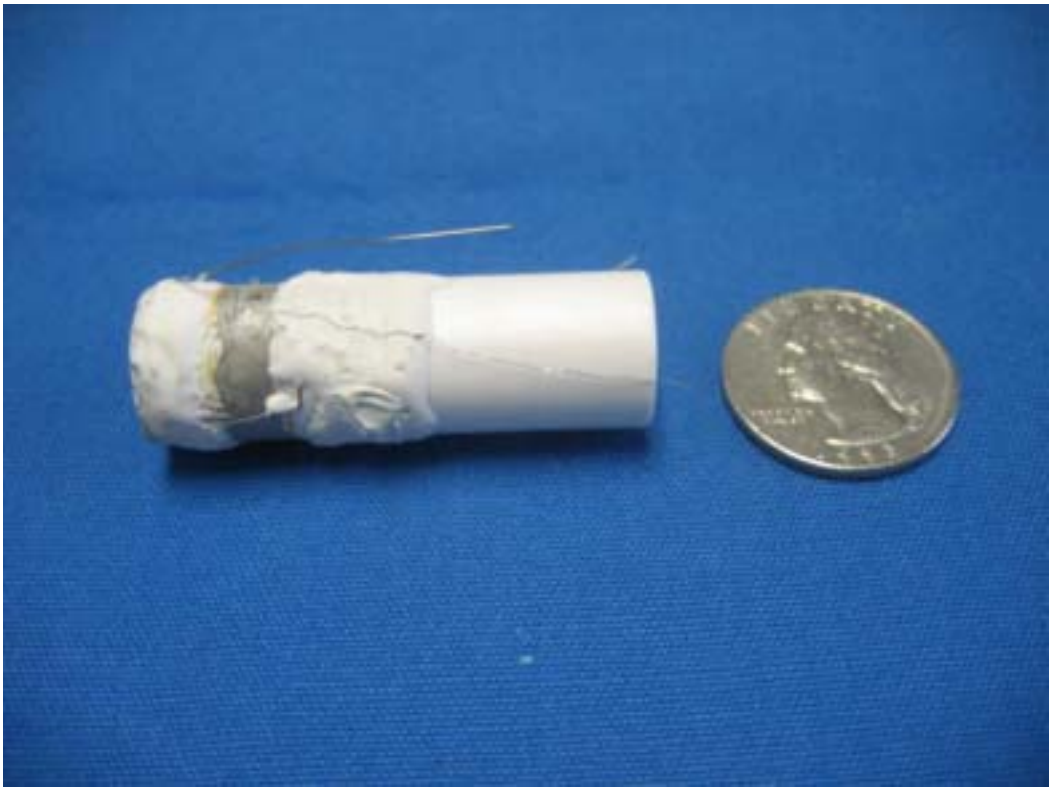

Figure V-5

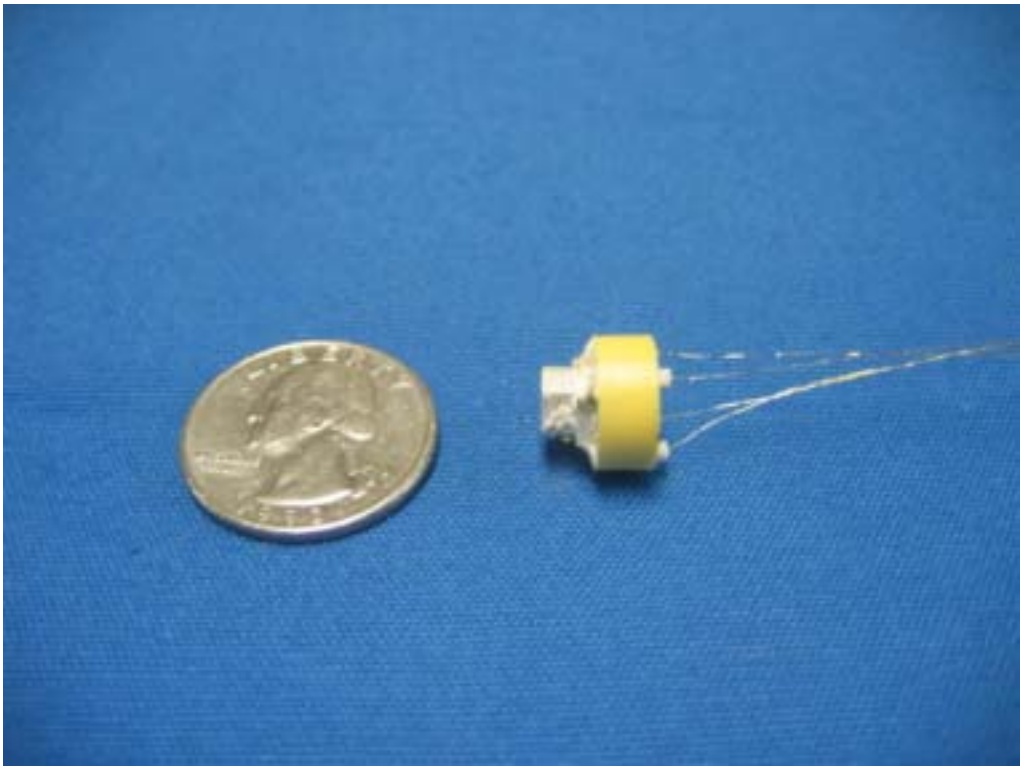

Figure V-6

Figure V-6 shows the stacked NO_x and O_2 sensors bonded to each other and the feedthru plug. Wires from the sensors extend thru the plug and are insulated by 1/16" o.d. mullite tubes shown extending to the right. Not shown is the thermocouple which will be bonded into the center well of the plug. An open hole in the plug (not seen) is used by the interior oxygen pumping lead.

It took a while to learn how to wind the heater. The problem was solved with the holder shown in Fig. V-7. Originally this jig was to be used to wind the heater onto the shell. This proved impractical because of the stiffness of the wire, so the two supports made of angled aluminum in front and back were added. These serve as clamps for the ends of the wire. After the heater is approximately preformed around a mandrel, including the bridge over the electrode, the wire is slipped over the shell, the ends are clamped and the wire is pulled tight and positioned correctly . In practice, the windings align properly on about half the shell and this side is potted with the Aremco material and fired. The other half of the windings are then more easily aligned properly and potted.

After winding and potting the heater coil, the sensor is assembled from the inside out. The sensors are bonded to the feedthru plug and wires are attached to sensors, fed thru the appropriate holes and sealed into the holes with the Aremco material (see Fig. V-6). The leads are long enough that they extend a little beyond the end of the shell when the plug is mounted into the shell. The thermocouple is attached at the same time. Wires to the pumping surface inside and outside the shell are also attached.

Next both plugs are mounted into the shell and bonded into place with the Aremco material. Lead extensions are attached to all wires using Engelhard gold paste. The extension wires for the heater are attached using crimp connectors. All the wires are insulated with the 1/16" o.d. mullite tubes. All 14 extension wires are fed thru the stainless steel extension tube and the stainless tube and the zirconia shell are attached using Aremco material.

Figure V-8 shows a fully-assembled sensor with insulation around the shell, insulated outer wires feeding into the opening in the stainless tube, a mounting flange for the test system at CeramPhysics, and lead junctions for the wires after they exit the stainless tube.

Although the assembly method above appears straightforward, there were multiple small problems that had to be solved, including the order of particular steps and providing more robust lead attachments at various points. Once assembled, a failure in any lead was impossible to fix and it was necessary to start over in the assembly process. There was only a limited number of steps that could be done on multiple sensors in parallel until the assembly methods had been tested and found adequate. Thus it took months to work out all the problems to the point where all subsystems of the sensor could be tested.

Two problems in particular caused problems. The first was learning how to mechanically anchor the leads inside the assembly, especially the leads to the sensors and the pumping surface. Eventually these problems were solved by changing the order of particular assembly steps, using thicker wires (even though they were harder to work with), and by finding additional anchor points for the leads, with the anchors provided by the Aremco material.

A particularly troublesome problem was multiple failures of the pumping lead attached to the inside of the shell. There was no adequate way to mechanically anchor the wire on the inside and there was too much stress and work-hardening of this wire as it was fed thru the feed-thru plug and extension leads were attached. This problem was eventually solved by firing a platinum track from the inner pumping surface along the interior of the shell (under the bonded feed-thru

Figure V-7

Figure V-8

plug) to near the end of the shell. At this point there was much more room for a mechanical anchors (using the Aremco material) and much less handling of the wire.

The second problem was more serious and involved the stack of the two sensors on the feedthru plug (see Fig. V-6). Originally silver wires were used to contact the pads on the sensor electrodes. They were fed through the holes in the feed-thru plug and anchored in place with a small amount of Aremco. The wires were bent to be in contact with the Pt/Au pads previously fired onto the sensors. A thicker layer of Au paste was added to join the wire to the sensor and was then fired. When the assembly was removed from the oven, there had often (but not always) been some kind of chemical reaction resulting in a yellow powder covering the wires, reacting with them and weakening them to the point of failure. At first, oven contamination was suspected, but that was eliminated. The assembly method was repeated with larger diameter Ag wires, but the results were still the same.

Eventually it was found that the reaction was between the silver and some material evolving from the Aremco at the high firing temperature required for the gold paste. The reaction occurred after the Aremco had been fully cured, but during the lead-attachment step between the Ag wire and the sensor. Ultimately the problem was solved by using gold wire instead of silver for the first section of the leads. The lead extensions discussed above were still Ag.

Tests of the Fully-Assembled Sensor

As the problems described above were being solved with multiple iterations of the assembly, there were some assemblies that could be partially tested. That is, some sub-systems in some assemblies worked and testing these sometimes identified additional assembly problems that needed to be solved. In particular, the heater/thermocouple controller sub-system usually worked well enough in the initial assemblies to test it. This testing identified an interaction between the temperature measurement system and the heater control. Previous tests of the controller had not been enough to identify the problem, and it took multiple tests of the assembly with the controller to narrow down the problem and identify the source. Once this problem was solved, it was found that the controller did a very good job of controlling the temperature of the assembly.

Near the end of the program, a couple of assemblies were made which initially had all the sub-systems working. However, a couple of these failed after limited testing due to lead failures.

Finally, a couple of other assemblies worked and could be tested. The first step was to test the heater control and to get an approximate calibration of both the NO_x and oxygen sensor. Both preliminary tests were successful. The final preliminary test was to evaluate the oxygen pump and controller. This was a subsystem that had not been previously tested with an oxygen sensor in place to evaluate the pump. With a gas containing 2% O_2/98% N_2, the pumping sub-system worked, but only marginally. The pump decreased the oxygen in the shell surrounding the sensors, but not by enough to make an accurate measurement of NO_x with the NO_x sensor. In addition, the oxygen pump controller would sometimes switch to a lower output. This switching caused fluctuations in the internal oxygen composition.

The basic cause of these problems was a combination of too large a porosity in the diffusion plug, and inadequate current output from the pumping controller to compensate for the additional oxygen. Two additional tests confirmed this analysis. First, Aremco material was added to the surface of the diffusion plug to further limit the gas flow into the sensor. This helped, but not enough. Second, a separate power supply with a larger voltage/current output than was

available from the controller was applied to the pumping surface. In this case, the oxygen inside the shell dropped to the tens of ppm range and could be held there steadily.

To eliminate these problems by obtaining diffusion plugs with lower porosity and increasing the output of the O_2 pump controller was beyond the time and money constraints remaining in the program.

Fully-Assembled Sensor Conclusions

As a conclusion, all the subsystems of the fully-assembled sensor worked, proving the concept. However, the pumping system sub-assembly was inadequate to claim complete success. Between the large residual oxygen content inside the shell and the oscillations from the controller, it was not possible to send any fully-assembled sensors to outside organizations for testing.

Tests at Sensata and Suggested Design Changes for the Future

In the early fall of 2007, Sensata Technologies of Attleboro, MA developed an interest in the sensor because their development group had been mandated by their management to identify and develop an automotive NO_x sensor. Sensata is a spinoff of Texas Instruments and has extensive and sophisticated testing and prototyping capabilities. Over the next few months Sensata purchased a number of NO_x and oxygen sensors made for them by MRA Labs. They also began developing their own "fully-assembled sensor" in addition to testing individual sensor bodies.

As stated in the letter from Sensata at the beginning of this report, they confirmed CeramPhysics measurements of the sensitivity of the sensor body and saw several advantages to the sensor over other possible sensors that they had identified. These advantages included the large sensitivity and the cost savings of using multilayer capacitor manufacturing methods. The disadvantage of the sensor was the need to develop a "reliable and cost-effective package" (quoting from their letter).

Their development path for the fully-assembled sensor was based on designs they had previously used with other sensors, and was a variation of a possible design suggested in Phase I of the program by CeramPhysics. This consisted of mounting the sensors on the hot end of a thin substrate (zirconia or alumina) which extended from the cold end to the hot end of the sensor. Leads to the sensors would be laid down as metal tracks on the substrate. A conceptual drawing is shown in Fig. V-9. A thin film heater would be printed on the back side of the substrate (not shown). Also not shown is a cover over the sensors in which the diffusion plug and oxygen pumping surface are located. The label in Fig. V-9 marked as "Problem Area for Interconnect" had been identified as a problem area by Sensata which needed to be solved before large quantities of inexpensive, reliable sensors could be manufactured. The drawing, along with some manufacturing suggestions (not elaborated on here), were a possible solution identified by CeramPhysics.

Besides the sensitivity tests Sensata performed, they were scheduled to perform a number of other tests, including but not limited to, cross-sensitivity tests to the other gases that would normally be in an automobile exhaust. However, before they were able to perform these tests, their management stopped all development of NO_x sensors because of the recent economic turndown in the auto industry.

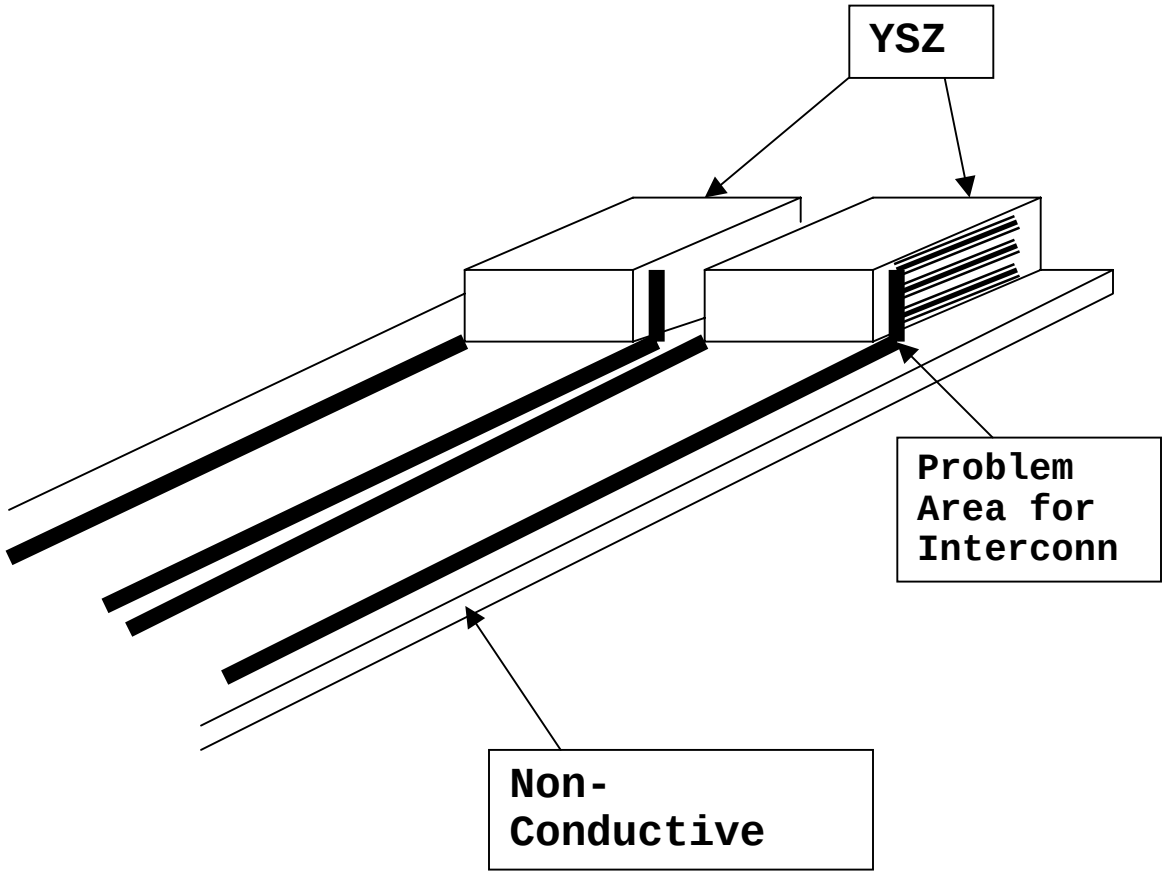

Figure V-9